A LOWEST-DEGREE STRICTLY CONSERVATIVE FINITE ELEMENT SCHEME FOR INCOMPRESSIBLE STOKES PROBLEM ON GENERAL TRIANGULATIONS

WENJIA LIU AND SHUO ZHANG

Abstract. In this paper, we propose a finite element pair for incompressible Stokes problem. The pair uses a slightly enriched piecewise linear polynomial space for velocity and piecewise constant space for pressure, and is illustrated to be a lowest-degree conservative stable pair for the Stokes problem on general triangulations.

1. Introduction

For the Stokes problem, if a stable finite element pair can inherit the mass conservation, the approximation of the velocity can be independent of the pressure and the method does not suffer from the locking effect with respect to large Reynolds' numbers (cf., e.g., [6]). Over the past decade, the conservative schemes have been recognized more clearly as *pressure robustness* and widely studied and surveyed in, e.g., [9, 11, 18, 23]. This conservation is also connected to other key features like "viscosity-independent" [27], "gradient-robustness" [19], etc for numerical schemes. The importance of conservative schemes is also significant in, e.g., the nonlinear mechanics [4, 5] and the magnetohydrodynamics [14-16]. Wide interests have been drawn to conservative schemes.

Various conservative finite element pairs have been designed for the Stokes problem. Conforming examples include conforming elements designed for special meshes, such as $\underset{\sim}{P}_k - P_{k-1}$ triangular elements for $k \geqslant 4$ on singular-vertex-free meshes [24] and for smaller k constructed on composite grids [3, 22, 24, 29, 32] and the pairs given in [8, 11] which work for general triangulations and with extra smoothness requirement. An alternative method is to use $H(\mathrm{div})$-conforming but H^1-nonconforming space for the velocity. A systematic approach is to add bubble-like functions onto $H(\mathrm{div})$ finite element spaces for the tangential weak continuity for the velocity. Examples along this line can be found in, e.g., [10, 20, 26] and [28]. Generally, to construct a conservative pair that works on general triangulations without special structures, cubic and higher-degree polynomials are used for the velocity.

2000 *Mathematics Subject Classification.* Primary 65N12, 65N15, 65N22, 65N30, 76D05.

Key words and phrases. Incompressible Stokes equations, inf-sup condition, conservative scheme, pressure-robust discretization, lowest degree.

The research is supported by NSFC (11871465) and CAS (XDB 41000000).

Recently, a new $\underset{\sim}{P}_2 - P_1$ finite element pair is proposed on general triangulations; for the velocity field, it uses piecewise quadratic $H(\mathrm{div})$ functions with enhanced tangential continuity, and for the pressure, it uses discontinuous piecewise linear functions. The pair is stable and immediately strictly conservative on general triangulations, and is of the lowest degree ever known. Meanwhile, as is pointed out in [30], this $\underset{\sim}{P}_2 - P_1$ pair can be viewed as a smoothened reduction from the famous Brezzi-Douglas-Marini pair, and this idea can be carried on for other $H(\mathrm{div})$ pairs so that the degree of finite element pairs may be reduced further.

In this paper, we study how low can the degree of polynomials be to construct a stable conservative pair that works on general triangulations. We begin with the reduction of the 2nd order Brezzi-Douglas-Fortin-Marini element pair to construct an auxiliary finite element pair $\underset{\sim}{V}_{h0}^{\mathrm{sBDFM}} - \mathbb{P}_{h0}^1$, and then a further reduction of the $\underset{\sim}{V}_{h0}^{\mathrm{sBDFM}} - \mathbb{P}_{h0}^1$ pair leads to a $\underset{\sim}{V}_{h0}^{\mathrm{el}} - \mathbb{P}_{h0}^0$ pair. The finally proposed pair, as the centerpiece of this paper, uses a slightly enriched linear polynomial space for the velocity and piecewise constant for the pressure, and is stable and conservative. A further reduction of this pair leads to a $\underset{\sim}{P}_1 - P_0$ pair which is constructed naturally but not stable on general triangulations, and this way we find the newly designed $\underset{\sim}{V}_{h0}^{\mathrm{el}} - \mathbb{P}_{h0}^0$ pair is one of lowest degree. We note that this $\underset{\sim}{V}_{h0}^{\mathrm{el}} - \mathbb{P}_{h0}^0$ pair is of the type "nonconforming spline" and can not be represented by Ciarlet's triple. However, the velocity space does admit a set of basis functions with quite tight local supports, which are clearly stated in Section 5.

The main technical ingredients of the paper are two folded. One is to figure out the basis functions, the supports of which are quite different from existing finite elements. Another is to prove the stability (inf-sup condition). We mainly utilize a two-step argument. For the auxiliary pair $\underset{\sim}{V}_{h0}^{\mathrm{sBDFM}} - \mathbb{P}_{h0}^1$, we mainly utilize Stenberg's macroelement argument by following the procedures of [30]; then the stability of the pair $\underset{\sim}{V}_{h0}^{\mathrm{el}} - \mathbb{P}_{h0}^0$, which is a sub-pair of $\underset{\sim}{V}_{h0}^{\mathrm{sBDFM}} - \mathbb{P}_{h0}^1$, is proved just by inheriting the stability of the $\underset{\sim}{V}_{h0}^{\mathrm{sBDFM}} - \mathbb{P}_{h0}^1$. This "reduce and inherit" procedure can be found in, e.g., [36, 37] where some low degree optimal schemes are designed for other problems. It can be a natural idea to generalize all technical ingredients here to other applications.

The rest of the paper is organized as follows. In the remaining of this section, we present some standard notations. Some preliminaries on finite elements are surveyed in Section 2. In Section 3, a smoothened BDFM element and an auxiliary stable conservative pair $\underset{\sim}{V}_{h0}^{\mathrm{sBDFM}} - \mathbb{P}_{h0}^1$, are established. In Section 4, a low-degree continuous nonconforming scheme for the biharmonic equation is presented. In Section 5, a low-degree stable conservative pair $\underset{\sim}{V}_{h0}^{\mathrm{el}} - \mathbb{P}_{h0}^0$ is constructed, while it is verified numerically in Appendix A that a further reduction of the degree leads to an

unstable pair. In Section 6, some numerical experiments are reported to illustrate the effect of the schemes given in the present paper. Finally, in Section 7, some concluding remarks are given.

1.1. **Notations.** In what follows, we use Ω to denote a simply connected polygonal domain. We use ∇, curl, div, rot, and ∇^2 to denote the gradient operator, curl operator, divergence operator, rot operator, and Hessian operator, respectively. As usual, we use $H^2(\Omega)$, $H_0^2(\Omega)$, $H^1(\Omega)$, $H_0^1(\Omega)$, $H(\mathrm{rot},\Omega)$, $H_0(\mathrm{rot},\Omega)$, and $L^2(\Omega)$ to denote certain Sobolev spaces, and specifically, denote $L_0^2(\Omega) := \{w \in L^2(\Omega) : \int_\Omega w dx = 0\}$, $\underset{\sim}{H}_0^1(\Omega) := (H_0^1(\Omega))^2$. Furthermore, we denote vector-valued quantities by "$\underset{\sim}{\cdot}$", while $\underset{\sim}{v}^1$ and $\underset{\sim}{v}^2$ denote the two components of the function $\underset{\sim}{v}$. We use $(\cdot,\cdot)$ to represent L^2 inner product, and $\langle\cdot,\cdot\rangle$ to denote the duality between a space and its dual. Without ambiguity, we use the same notation $\langle\cdot,\cdot\rangle$ for different dualities, and it can occasionally be treated as L^2 inner product for certain functions. We use the subscript " $\cdot_h$ " to denote the dependence on triangulation. In particular, an operator with the subscript " $\cdot_h$ " indicates that the operation is performed cell by cell. Finally, $\underset{\sim}{=}$ denotes equality up to a constant. The hidden constants depend on the domain, and when triangulation is involved, they also depend on the shape regularity of the triangulation, but they do not depend on h or any other mesh parameter.

The two complexes below are well known.

$$\{0\} \xrightarrow{\mathrm{inc}} H_0^1(\Omega) \xrightarrow{\mathrm{curl}} H_0(\mathrm{div},\Omega) \xrightarrow{\mathrm{div}} L_0^2(\Omega) \xrightarrow{\int_\Omega \cdot} \{0\}, \tag{1.1}$$

$$\{0\} \xrightarrow{\mathrm{inc}} H_0^2(\Omega) \xrightarrow{\mathrm{curl}} \underset{\sim}{H}_0^1(\Omega) \xrightarrow{\mathrm{div}} L_0^2(\Omega) \xrightarrow{\int_\Omega \cdot} \{0\}. \tag{1.2}$$

We refer to, e.g., [1, 2] for related discussion on more complexes and finite elements.

The fundamental incompressible Stokes problem reads:

$$\begin{cases} -\varepsilon^2 \Delta \underset{\sim}{u} + \nabla p = \underset{\sim}{f}, & \text{in } \Omega, \\ \mathrm{div}\, \underset{\sim}{u} = 0, & \text{in } \Omega, \\ \underset{\sim}{u} = \underset{\sim}{0}, & \text{on } \partial\Omega. \end{cases} \tag{1.3}$$

Here $\underset{\sim}{u}$ stands for the velocity field and p for the pressure field of the incompressible flow, and ε^2 stands for the inverse of the Reynold's number, which can be very small. Its variational formulation is to find $(\underset{\sim}{u}, p) \in \underset{\sim}{H}_0^1(\Omega) \times L_0^2(\Omega)$, such that

$$\begin{cases} \varepsilon^2(\nabla \underset{\sim}{u}, \nabla \underset{\sim}{v}) - (\mathrm{div}\, \underset{\sim}{v}, p) &= (\underset{\sim}{f}, \underset{\sim}{v}), \quad \forall\, \underset{\sim}{v} \in \underset{\sim}{H}_0^1(\Omega), \\ (\mathrm{div}\, \underset{\sim}{u}, q) &= 0, \qquad \forall\, q \in L_0^2(\Omega). \end{cases} \tag{1.4}$$

2. Preliminaries

2.1. **Triangulations.** Let $\mathcal{T}_h$ be a shape-regular triangular subdivision of Ω with mesh size h, such that $\overline{\Omega} = \cup_{T\in\mathcal{T}_h}\overline{T}$. Denote by $\mathcal{T}_h$, $\mathcal{T}_h^i$, $\mathcal{E}_h$, $\mathcal{E}_h^i$, $\mathcal{E}_h^b$, $\mathcal{X}_h$, $\mathcal{X}_h^i$ and $\mathcal{X}_h^b$ the set of cells, cells with three interior edges, edges, interior edges, boundary edges, vertices, interior vertices and boundary vertices, respectively. For any edge $e \in \mathcal{E}_h$, denote by $\mathbf{n}_e$ and $\mathbf{t}_e$ the unit normal and tangential vectors of e, respectively. The subscript $\cdot_e$ can be dropped when there is no ambiguity.

Denote

$$\mathcal{X}_h^{b,+1} := \{a \in \mathcal{X}_h^i,\ a \text{ is connected to } \mathcal{X}_h^b \textit{ by } e \in \mathcal{E}_h^i\}, \text{ and } \mathcal{X}_h^{i,-1} := \mathcal{X}_h^i \setminus \mathcal{X}_h^{b,+1};$$

further, denote with $\mathcal{X}_h^{i,-(k-1)} \neq \emptyset$,

$$\mathcal{X}_h^{b,+k} := \{a \in \mathcal{X}_h^{i,-(k-1)},\ a \text{ is connected to } \mathcal{X}_h^{b,+(k-1)} \textit{ by } e \in \mathcal{E}_h^i\}, \text{ and } \mathcal{X}_h^{i,-k} := \mathcal{X}_h^{i,-(k-1)} \setminus \mathcal{X}_h^{b,+k}.$$

The smallest k such that $\mathcal{X}_h^{i,-(k-1)} = \mathcal{X}_h^{b,+k}$ is called the number of layers of the triangulation.

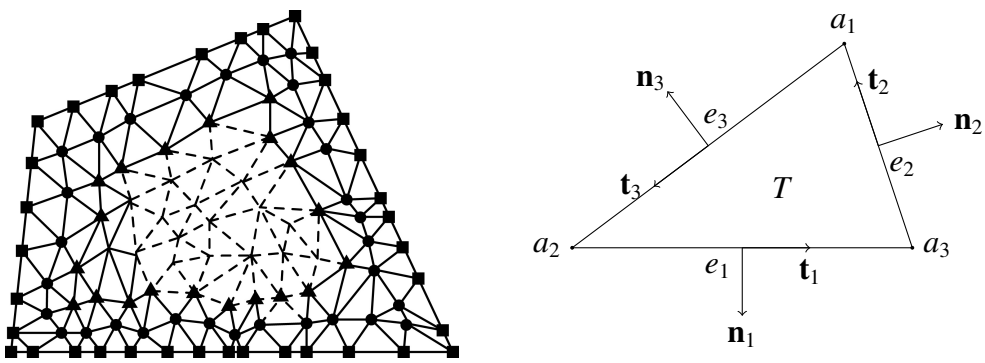

Figure 1. Left: vertex layers, where the ■'s denote boundary vertices, the •'s denote vertices of $\mathcal{X}_h^{b,+1}$, the ▲'s denote vertices of $\mathcal{X}_h^{b,+2}$, and so forth. Right: a reference triangle.

On a triangle T, locally we use $\{a_1, a_2, a_3\}$ to denote its three vertices and $\{e_1, e_2, e_3\}$ to denote three edges with unit outward normal vectors $\{\mathbf{n}_1, \mathbf{n}_2, \mathbf{n}_3\}$ and unit tangential vectors $\{\mathbf{t}_1, \mathbf{t}_2, \mathbf{t}_3\}$ such that $\mathbf{n}_i \times \mathbf{t}_i > 0, i \in \{1, 2, 3\}$; see Figure 1(right) for an illustration. In addition $\{\lambda_1, \lambda_2, \lambda_3\}$ are the barycentric coordinates with respect to the three corners of T. Also denote the lengths of edges by $\{d_1, d_2, d_3\}$, and the area of T by S_T and drop the subscript when no ambiguity is brought in.

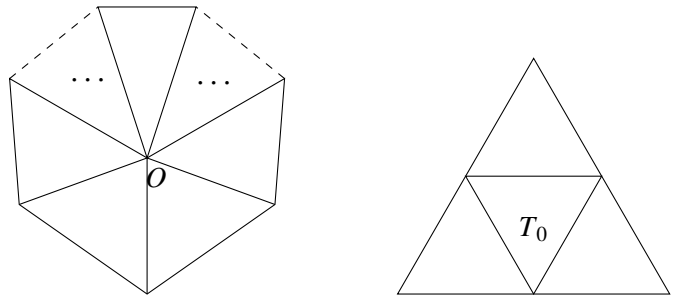

FIGURE 2. Illustration of an interior vertex patch(left) and an interior cell patch(right).

Next, we figure out two types of patches.

interior vertex patch:: for an interior vertex O, the cells that connects to O form a (closed) interior vertex patch, denoted by P_O; see Figure 2(left) for an illustration;

interior cell patch:: for an interior cell T_0, three neighbored cells and T_0 form an interior cell patch, denoted by P_{T_0}; see Figure 2(right) for an illustration.

The number of interior vertex patches is $\#\mathcal{X}_h^i$ and the number of interior cell patches is $\#\mathcal{T}_h^i (= 2\#\mathcal{X}_h^i - 2)$.

In the sequel, we impose a mild assumption on the grid.

Assumption 1. *Every boundary vertex is connected to at least one interior vertex.*

This assumption assures every cell is covered by at least one interior vertex patch.

2.2. **Polynomial spaces on a triangle.** For a triangle T, we use $P_k(T)$ to denote the set of polynomials on K of degrees not higher than k. In a similar manner, $P_k(e)$ is defined on an edge e. We define $\underset{\sim}{P}_k(T) = (P_k(T))^2$ and similarly is $\underset{\sim}{P}_k(e)$ defined.

Following [20], we introduce the shape function space:

$$\underset{\sim}{P}^{\mathrm{MTW}}(T) := \{\underset{\sim}{v} \in \underset{\sim}{P}_3(T) : \underset{\sim}{v} \cdot \mathbf{n}|_{e_i} \in P_1(e_i),\ i = 1:3,\ \operatorname{div} \underset{\sim}{v} \text{ is a constant on } T\}.$$

It can be verified (cf. [10]) that

$$\underset{\sim}{P}^{\mathrm{MTW}}(T) = \underset{\sim}{P}_1(T) \oplus \operatorname{span}\{\operatorname{curl}(\lambda_i^2 \lambda_j \lambda_k)\}_{\{i,j,k\}=\{1,2,3\}}.$$

Following [10], we introduce the shape functions space

$$\underset{\sim}{P}^{\mathrm{GN}-1}(T) = \underset{\sim}{P}_1(T) \oplus \{\operatorname{curl}(\lambda_i^2 \lambda_j^2 \lambda_k)\}_{\{i,j,k\}=\{1,2,3\}}.$$

We further denote

$$\underset{\sim}{P}^{2-}(T) := \underset{\sim}{P}_1(T) \oplus \operatorname{span}\{\lambda_i \lambda_j \mathbf{t}_k\}_{\{i,j,k\}=\{1,2,3\}}, \quad \text{and} \quad \underset{\sim}{P}^{1+}(T) := \underset{\sim}{P}_1(T) \oplus \operatorname{span}\{\operatorname{curl}(\lambda_1 \lambda_2 \lambda_3)\}.$$

It can be verified that $\underset{\sim}{P}^{1+}(T) \subset \underset{\sim}{P}^{2-}(T)$, and

$$\underset{\sim}{P}^{2-}(T) = \{\underset{\sim}{v} \in \underset{\sim}{P}_2(T) : \underset{\sim}{v}\cdot\mathbf{n}|_{e_i} \in P_1(e_i),\ i = 1:3\}, \quad \text{and} \quad \underset{\sim}{P}^{1+}(T) = \{\underset{\sim}{v} \in \underset{\sim}{P}^{2-}(T) : \operatorname{div}\underset{\sim}{v} \text{ is a constant on } T\}.$$

Further we denote

$$P^{2+}(T) := P_2(T) \oplus \operatorname{span}\{\lambda_1\lambda_2\lambda_3\}.$$

Lemma 2.1. *The two exact sequences hold:*

$$\mathbb{R} \to P^{2+}(T) \xrightarrow{\text{curl}} \underset{\sim}{P}^{2-}(T) \xrightarrow{\text{div}} P_1(T), \tag{2.1}$$

and

$$\mathbb{R} \to P^{2+}(T) \xrightarrow{\text{curl}} \underset{\sim}{P}^{1+}(T) \xrightarrow{\text{div}} P_0(T). \tag{2.2}$$

Proof. Noting that $\underset{\sim}{P}^{2-}(T)$ is exactly the local shape functions space of the quadratic Brezzi-Douglas-Fortin-Marini element, that $\operatorname{div}\underset{\sim}{P}^{2-}(T) = P_1(T)$ is well known. Evidently $\operatorname{curl} P^{2+}(T) \subset \{\underset{\sim}{v} \in \underset{\sim}{P}^{2-}(T) : \operatorname{div}\underset{\sim}{v} = 0\}$, and $\dim(\operatorname{curl} P^{2+}(T)) = \dim(P^{2+}(T)) - 1 = \dim(\underset{\sim}{P}^{2-}(T)) - \dim(P_1(T)) = \dim(\{\underset{\sim}{v} \in \underset{\sim}{P}^{2-}(T) : \operatorname{div}\underset{\sim}{v} = 0\})$, thus $\operatorname{curl} P^{2+}(T) = \{\underset{\sim}{v} \in \underset{\sim}{P}^{2-}(T) : \operatorname{div}\underset{\sim}{v} = 0\}$. The proof of (2.1) is completed. Similarly, that $\operatorname{div}\underset{\sim}{P}^{1+}(T) = P_0(T)$ follows by the definition of $\underset{\sim}{P}^{1+}(T)$, and (2.2) can be proved the same way. □

Define for $i = 1:3$, $\underset{\sim}{w}_{T,e_i} := \operatorname{curl}(\lambda_j\lambda_k(3\lambda_i - 1))$, $\underset{\sim}{w}_{T,e_j,e_k} := \operatorname{curl}(\lambda_i^2)$ and $\underset{\sim}{y}_{T,e_j,e_k} := -\frac{2}{d_i}\lambda_i\mathbf{n}_i$. It holds trivially that $\operatorname{div}\underset{\sim}{w}_{T,e_i} = 0$, $\operatorname{div}\underset{\sim}{w}_{T,e_j,e_k} = 0$ and $\operatorname{div}\underset{\sim}{y}_{T,e_j,e_k} = \frac{1}{S}$. It also indicates that $\underset{\sim}{w}_{T,e_i}$ is a function with vanishing normal components and tangential integral on the edges e_j, e_k and similar is $\underset{\sim}{w}_{T,e_j,e_k}$ on the edge e_i. For instance, we refer to Figure 3 for an illustration of $\underset{\sim}{w}_{T,e_1}$ and $\underset{\sim}{w}_{T,e_2,e_3}$.

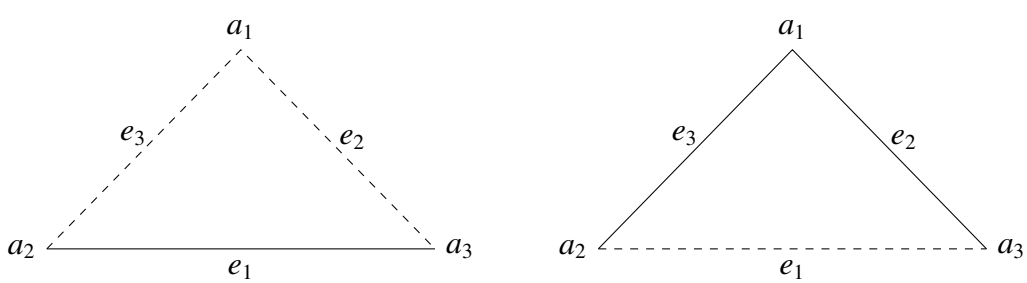

FIGURE 3. Degrees of freedom vanish on dotted edges.

Then

$$\begin{aligned}\underset{\sim}{Z}_T := \{\underset{\sim}{v} \in \underset{\sim}{P}^{2-}(T) : \operatorname{div}\underset{\sim}{v} = 0\} &= \{\underset{\sim}{v} \in \underset{\sim}{P}^{1+}(T) : \operatorname{div}\underset{\sim}{v} = 0\} \\ &= \operatorname{span}\{\underset{\sim}{w}_{T,e_1}, \underset{\sim}{w}_{T,e_2}, \underset{\sim}{w}_{T,e_3}, \underset{\sim}{w}_{T,e_2,e_3}, \underset{\sim}{w}_{T,e_3,e_1}, \underset{\sim}{w}_{T,e_1,e_2}\}\end{aligned} \tag{2.3}$$

and

$$\underset{\sim}{P}^{1+}(T) = \text{span}\{\underset{\sim}{w}_{T,e_1}, \underset{\sim}{w}_{T,e_2}, \underset{\sim}{w}_{T,e_3}, \underset{\sim}{w}_{T,e_2,e_3}, \underset{\sim}{w}_{T,e_3,e_1}, \underset{\sim}{w}_{T,e_1,e_2}, \underset{\sim}{y}_{T,e_2,e_3}, \underset{\sim}{y}_{T,e_3,e_1}, \underset{\sim}{y}_{T,e_1,e_2}\}. \tag{2.4}$$

Indeed, the functions of the set in (2.4) are not linearly independent. Any one among $\{\underset{\sim}{y}_{T,e_2,e_3}, \underset{\sim}{y}_{T,e_3,e_1}, \underset{\sim}{y}_{T,e_1,e_2}\}$ together with $\{\underset{\sim}{w}_{T,e_1}, \underset{\sim}{w}_{T,e_2}, \underset{\sim}{w}_{T,e_3}, \underset{\sim}{w}_{T,e_2,e_3}, \underset{\sim}{w}_{T,e_3,e_1}, \underset{\sim}{w}_{T,e_1,e_2}\}$ forms a set of independent basis of $\underset{\sim}{P}^{1+}(T)$.

2.3. **Some known finite elements.** The Madal-Tai-Winther element (see [20]) is defined by

(1) T is a triangle;
(2) $P_T = \underset{\sim}{P}^{MTW}(T)$;
(3) for any $\underset{\sim}{v} \in (H^1(T))^2$, the nodal parameters on T, denoted by D_T, are
$\{\fint_{e_i} \underset{\sim}{v} \cdot \mathbf{n}_{T,e_i} d\tau, \fint_{e_i} \underset{\sim}{v} \cdot \mathbf{n}_{T,e_i}(\lambda_j - \lambda_k) d\tau, \fint_{e_i} \underset{\sim}{v} \cdot \mathbf{t}_{T,e_i} d\tau\}_{i=1:3}$.

Following [20], introduce

$$\underset{\sim}{V}_h^{\text{MTW}} := \{\underset{\sim}{v}_h \in H(\text{div}, \Omega) : \underset{\sim}{v}_h|_T \in \underset{\sim}{P}^{\text{MTW}}(T), \ \int_e \underset{\sim}{v} \cdot \mathbf{t} \text{ is continuous across interior edge } e\}, \tag{2.5}$$

and

$$\underset{\sim}{V}_{h0}^{\text{MTW}} := \{\underset{\sim}{v}_h \in \underset{\sim}{V}_h^{\text{MTW}} \cap H_0(\text{div}, \Omega) : \ \int_e \underset{\sim}{v} \cdot \mathbf{t} = 0 \text{ on boundary edge } e\}. \tag{2.6}$$

The lowest-degree Guzman-Neilan element (see [10]) is defined as

(1) T is a triangle;
(2) $P_T = \underset{\sim}{P}^{\text{GN}-1}(T)$;
(3) for any $\underset{\sim}{v} \in (H^1(T))^2$, the nodal parameters on T, denoted by D_T, are
$\{\fint_{e_i} \underset{\sim}{v} \cdot \mathbf{n}_{T,e_i} d\tau, \fint_{e_i} \underset{\sim}{v} \cdot \mathbf{n}_{T,e_i}(\lambda_j - \lambda_k) d\tau, \fint_{e_i} \underset{\sim}{v} \cdot \mathbf{t}_{T,e_i} d\tau\}_{i=1:3}$.

Following [10], introduce

$$\underset{\sim}{V}_h^{\text{GN}-1} := \{\underset{\sim}{v}_h \in H(\text{div}, \Omega) : \underset{\sim}{v}_h|_T \in P^{\text{GN}-1}(T), \ \int_e \underset{\sim}{v} \cdot \mathbf{t} \text{ is continuous across interior edge } e\}, \tag{2.7}$$

and

$$\underset{\sim}{V}_{h0}^{\text{GN}-1} := \{\underset{\sim}{v}_h \in \underset{\sim}{V}_h^{\text{GN}-1} \cap H_0(\text{div}, \Omega) : \ \int_e \underset{\sim}{v} \cdot \mathbf{t} = 0 \text{ on boundary edge } e\}. \tag{2.8}$$

Following Zeng-Zhang-Zhang [30], introduce

$$\underset{\sim}{V}_h^{\text{ZZZ}} := \{\underset{\sim}{v}_h \in H(\text{div}, \Omega) : \underset{\sim}{v}_h|_T \in \underset{\sim}{P}_2(T), \ \int_e \underset{\sim}{v} \cdot \mathbf{t} \text{ is continuous across interior edge } e\}, \tag{2.9}$$

and

$$\underset{\sim}{V}_{h0}^{ZZZ} := \{\underset{\sim}{v}_h \in \underset{\sim}{V}_h^{ZZZ} \cap H_0(\mathrm{div}, \Omega) : \int_e \underset{\sim}{v} \cdot \mathbf{t} = 0 \text{ on boundary edge } e\}. \tag{2.10}$$

As revealed by [30], the space can be viewed as a reduced Brezzi-Douglas-Marini element space with enhanced smoothness.

2.4. **Stenberg's macroelement technique for inf-sup condition (cf. [25]).** A macroelement partition of $\mathcal{T}_h$, denoted by $\mathcal{M}_h$, is a set of macroelements satisfying that each triangle of $\mathcal{T}_h$ is covered by at least one macroelement in $\mathcal{M}_h$.

Definition 2.2. *Two macroelements M_1 and M_2 are said to be equivalent if there exists a continuous one-to-one mapping $G : M_1 \to M_2$, such that*

(a) $G(M_1) = M_2$

(b) if $M_1 = \bigcup_{i=1:m}^{m} T_i^1$, then $T_i^2 = G(T_i^1)$ with $i = 1 : m$ are the cells of M_2.

(c) $G|_{T_i^1} = F_{T_i^2} \circ F_{T_i^1}^{-1}, i = 1 : m$, where $F_{T_i^1}$ and $F_{T_i^2}$ are the mappings from a reference element $\hat{T}$ onto T_i^1 and T_i^2, respectively.

A class of equivalent macroelements is a set of which any two macroelements are equivalent to each other. Given a macroelement M, $\underset{\sim}{V}_{h0,M}$, a subspace of $\underset{\sim}{V}_h$, consists of functions in $\underset{\sim}{V}_h$ that are equal to zero outside M; continuity constraints of $\underset{\sim}{V}_h$ enable corresponding nadal parameters of functions in $\underset{\sim}{V}_{h0,M}$ to be zero on ∂M. Similarly, $Q_{h,M}$ is a subspace of Q_h and it consists of functions that are equal to zero outside M. Denote

$$N_M := \{q_h \in Q_{h,M} : \int_M div\, \underset{\sim}{v}_h\, q_h\, dM = 0, \forall\, \underset{\sim}{v}_h \in \underset{\sim}{V}_{h0,M}\}. \tag{2.11}$$

Stenberg's macroelement technique can be summarized as the following proposition.

Proposition 2.3. *Suppose there exist a macroelement partitioning $\mathcal{M}_h$ with a fixed set of equivalence classes $\mathbb{E}_i$ of macroelements, $i = 1, 2, ..., n$, a positive integer N (n and N are independent of h), and an operator $\Pi : H_0^1(\Omega) \to \underset{\sim}{V}_{h0}$, such that*

(C_1) for each $M \in \mathbb{E}_i, i = 1, 2, ..., n$, the space N_M defined in (2.11) is one-dimensional, which consists of functions that are constant on M;

(C_2) each $M \in \mathcal{M}_h$ belongs to one of the classes $\mathbb{E}_i, i = 1, 2, ..., n$;

(C_3) each $e \in \mathcal{E}_h^i$ is an interior edge of at least one and no more than N macroelements;

(C_4) for any $\underset{\sim}{w} \in \underset{\sim}{H}_0^1(\Omega)$, it holds that

$$\sum_{T \in \mathcal{T}_h} h_T^{-2} \|\underset{\sim}{w} - \Pi \underset{\sim}{w}\|_{0,T}^2 + \sum_{e \in \mathcal{E}_h^i} h_e^{-1} \|\underset{\sim}{w} - \Pi \underset{\sim}{w}\|_{0,e}^2 \leqslant C \|\underset{\sim}{w}\|_{1,\Omega}^2 \quad \textit{and} \quad \|\Pi \underset{\sim}{w}\|_{1,h} \leqslant C \|\underset{\sim}{w}\|_{1,\Omega}.$$

Then the uniform inf-sup condition holds for the finite element pair.

3. An auxiliary stable pair for the Stokes problem

3.1. **A smoothened Brezzi-Douglas-Fortin-Marini** (sBDFM) **element.** We define sBDFM element by

(1) T is a triangle;

(2) $P_T = \underset{\sim}{P}^{2-}(T)$;

(3) for any $\underset{\sim}{v} \in (H^1(T))^2$, the nodal parameters on T, denoted by D_T, are

$$\{\fint_{e_i} \underset{\sim}{v} \cdot \mathbf{n}_{T,e_i} d\tau, \fint_{e_i} \underset{\sim}{v} \cdot \mathbf{n}_{T,e_i}(\lambda_j - \lambda_k) d\tau, \fint_{e_i} \underset{\sim}{v} \cdot \mathbf{t}_{T,e_i} d\tau\}_{i=1:3}.$$

The above triple is P_T-unisolvent. We use $\underset{\sim}{\varphi}_{\mathbf{n}_{T,e_i},0}$, $\underset{\sim}{\varphi}_{\mathbf{n}_{T,e_i},1}$, and $\underset{\sim}{\varphi}_{\mathbf{t}_{T,e_i},0}$ to represent the corresponding nodal basis functions, and then

$$\begin{cases} \underset{\sim}{\varphi}_{\mathbf{n}_{T,e_i},0} = \lambda_j(3\lambda_j - 2)\dfrac{\mathbf{t}_k}{(\mathbf{n}_i, \mathbf{t}_k)} + \lambda_k(3\lambda_k - 2)\dfrac{\mathbf{t}_j}{(\mathbf{n}_i, \mathbf{t}_j)} + 6\lambda_j\lambda_k\mathbf{n}_i; \\ \underset{\sim}{\varphi}_{\mathbf{n}_{T,e_i},1} = 3\lambda_j(3\lambda_j - 2)\dfrac{\mathbf{t}_k}{(\mathbf{n}_i, \mathbf{t}_k)} - 3\lambda_k(3\lambda_k - 2)\dfrac{\mathbf{t}_j}{(\mathbf{n}_i, \mathbf{t}_j)}; \\ \underset{\sim}{\varphi}_{\mathbf{t}_{T,e_i},0} = 6\lambda_j\lambda_k\mathbf{t}_i. \end{cases} \tag{3.1}$$

We use $\underset{\sim}{V}_h^{\text{sBDFM}}$ and $\underset{\sim}{V}_{h0}^{\text{sBDFM}}$ for the corresponding finite element spaces, where the subscript $\cdot_{h0}$ implies that the nodal parameters along boundary of the domain are all zero. Evidently, $\underset{\sim}{V}_h{}^{\text{sBDFM}}$ is a **s**moothened subspace of the famous Brezzi-Douglas-Fortin-Marini element space. Indeed $\underset{\sim}{V}_h^{\text{sBDFM}} \subset \underset{\sim}{H}(div, \Omega)$ but $\underset{\sim}{V}_h^{\text{sBDFM}} \not\subset \underset{\sim}{H}^1(\Omega)$, and similar is $\underset{\sim}{V}_{h0}^{\text{sBDFM}}$.

Define a nodal interpolation operator $\Pi_h : \underset{\sim}{H}^1(\Omega) \to \underset{\sim}{V}_h^{\text{sBDFM}}$ such that for any $e \subset \mathcal{E}_h$,

$$\fint_e (\Pi_h \underset{\sim}{v} \cdot \mathbf{n}_e) p = \fint_e (\underset{\sim}{v} \cdot \mathbf{n}_e) p, \ \forall\, p \in P_1(e) \quad \text{and} \quad \fint_e \Pi_h \underset{\sim}{v} \cdot \mathbf{t}_e = \fint_e \underset{\sim}{v} \cdot \mathbf{t}_e.$$

The operator Π_h is locally defined on each triangle, and it preserves linear functions locally. Furthermore, the local space $\underset{\sim}{V}_h(T)$ restricted on T is invariant under the Piola's transformation, i.e., it maps $\underset{\sim}{V}_h(T)$ onto $\underset{\sim}{V}_h(\hat{T})$. Therefore, approximation estimates of Π_h can be derived from standard scaling arguments and the Bramble-Hilbert lemma.

Proposition 3.1. *It holds for* $0 \le k \le 1 \le s \le 3$ *that*

$$|\underset{\sim}{v} - \Pi_h \underset{\sim}{v}|_{k,h} \leqslant C h^{s-k} |\underset{\sim}{v}|_{s,\Omega}, \quad \forall\, \underset{\sim}{v} \in \underset{\sim}{H}^s(\Omega). \tag{3.2}$$

3.2. **Structure of the kernel of** div **on a closed patch.** For an $m-$cell interior vertex patch P_O, we label cells of it sequentially as $T_i, i = 1 : m$, and label $e_i = \overline{T_i} \cap \overline{T_{i+1}}, i = 1 : m-1, e_m = \overline{T_m} \cap \overline{T_1}$. Also, we label $e_{m+i}, i = 1 : m$, the edge opposite O in T_i; see Figure 4 (left) for an illustration.

Viewing P_O as a special grid, we construct $\underset{\sim}{V}_{h0}^{\mathrm{sBDFM}}(P_O)$ thereon, and denote

$$\underset{\sim}{Z}_O := \{\underset{\sim}{v} \in \underset{\sim}{V}_{h0}^{\mathrm{sBDFM}}(P_O) : \operatorname{div} \underset{\sim}{v} = 0\}.$$

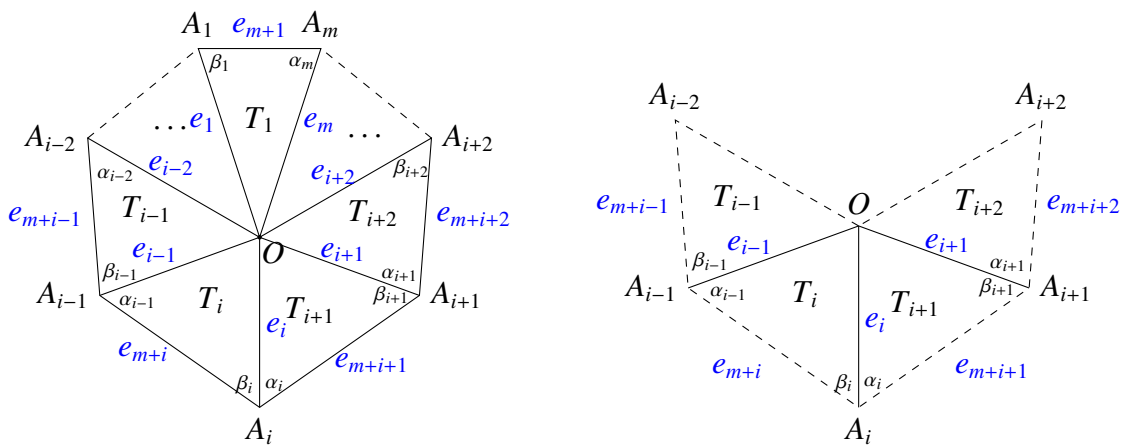

FIGURE 4. Illustration of a patch around O(left) and its part amplification(right).

Lemma 3.2. $\dim(\underset{\sim}{Z}_O) = 1$.

Proof. Assume $\underset{\sim}{\psi}_h \in \underset{\sim}{Z}_O$, then $\underset{\sim}{\psi}_h|_{T_i} \subset \underset{\sim}{Z}_{T_i}$, $i = 1 : m$. By the boundary conditions, it follows that

$$\underset{\sim}{\psi}_h|_{T_i} = \gamma_{T_i}^{i-1} \underset{\sim}{w}_{T_i,e_{i-1}} + \gamma_{T_i}^{i} \underset{\sim}{w}_{T_i,e_i} + \gamma_{T_i}^{i-1,i} \underset{\sim}{w}_{T_i,e_{i-1}e_i}, \tag{3.3}$$

with $\gamma_{T_i}^{i-1}$, $\gamma_{T_i}^{i}$ and $\gamma_{T_i}^{i-1,i}$ determined such that $\underset{\sim}{\psi}_h$ satisfies the continuity restriction of $\underset{\sim}{V}_h^{\mathrm{sBDFM}}$.

For an arbitrary edge e_i, $1 \leqslant i \leqslant m$, across it the normal component of $\underset{\sim}{\psi}_h$ and integration of the tangential component of $\underset{\sim}{\psi}_h$ are continuous; see Figure 4(right) for an illustration. Based on the continuity conditions, a direct calculation shows that

$$\begin{cases} \gamma_{T_i}^{i-1,i} = \gamma_{T_{i+1}}^{i,i+1}, \\ \gamma_{T_i}^{i} = \dfrac{d_{m+i} d_{m+i+1} \sin(\alpha_i + \beta_i)}{2(S_i + S_{i+1})} \gamma_{T_i}^{i-1,i}, \\ \gamma_{T_{i+1}}^{i} = \dfrac{d_{m+i} d_{m+i+1} \sin(\alpha_i + \beta_i)}{2(S_i + S_{i+1})} \gamma_{T_{i+1}}^{i,i+1}. \end{cases} \tag{3.4}$$

By checking all edges e_i, $i = 1 : m$, we have

$$\gamma_{T_1}^{m,1} = \gamma_{T_2}^{1,2} = \ldots = \gamma_{T_m}^{m-1,m}, \tag{3.5}$$

and

$$\begin{cases} \gamma_{T_i}^{i-1} = \dfrac{d_{m+i-1}d_{m+i}\sin(\alpha_{i-1}+\beta_{i-1})}{2(S_{i-1}+S_i)}\gamma_{T_i}^{i-1,i}, \\ \gamma_{T_i}^{i} = \dfrac{d_{m+i}d_{m+i+1}\sin(\alpha_i+\beta_i)}{2(S_i+S_{i+1})}\gamma_{T_i}^{i-1,i}. \end{cases} \tag{3.6}$$

In other words,

$$\begin{cases} \gamma_{T_1}^{m} = \dfrac{d_{2m}d_{m+1}\sin(\alpha_m+\beta_m)}{2(S_m+S_1)}\gamma_{T_1}^{m,1}, \\ \gamma_{T_i}^{i-1} = \dfrac{d_{m+i-1}d_{m+i}\sin(\alpha_{i-1}+\beta_{i-1})}{2(S_{i-1}+S_i)}\gamma_{T_i}^{i-1,i}\ (i=2:m), \end{cases} \tag{3.7}$$

and

$$\begin{cases} \gamma_{T_i}^{i} = \dfrac{d_{m+i}d_{m+i+1}\sin(\alpha_i+\beta_i)}{2(S_i+S_{i+1})}\gamma_{T_i}^{i-1,i}\ (i=1:m-1), \\ \gamma_{T_m}^{m} = \dfrac{d_{2m}d_{m+1}\sin(\alpha_m+\beta_m)}{2(S_m+S_1)}\gamma_{T_m}^{m-1,m}. \end{cases} \tag{3.8}$$

By the relations (3.5), (3.7) and (3.8), we can choose $\gamma_{T_1}^{m,1} = 1$, and other coefficients accordingly, then $\underset{\sim}{\psi}_h \in \underset{\sim}{Z}_O$, and moreover $\underset{\sim}{Z}_O = \mathrm{span}\{\underset{\sim}{\psi}_h\}$. The proof is completed. □

3.3. **A stable conservative pair for the Stokes problem.** Denote

$$\mathbb{P}_h^1(\mathcal{T}_h) := \{q_h \in L^2(\Omega) : q_h|_T \in P_1(T), \forall\, T \in \mathcal{T}_h\} \text{ and } \mathbb{P}_{h0}^1(\mathcal{T}_h) := \mathbb{P}_h^1(\mathcal{T}_h) \cap L_0^2(\Omega).$$

Then $\underset{\sim}{V}_{h0}^{\mathrm{sBDFM}} \times \mathbb{P}_{h0}^1$ forms a stable pair for the Stokes problem.

Theorem 3.3 (Inf-sup conditions)**.** *Let $\{\mathcal{T}_h\}$ be a family of triangulations of Ω satisfying* **Assumption 1**. *Then*

$$\sup_{\underset{\sim}{v}_h \in \underset{\sim}{V}_{h0}^{\mathrm{sBDFM}}} \frac{(div\ \underset{\sim}{v}_h, q_h)}{\|\underset{\sim}{v}_h\|_{1,h}} \geqslant C\|q_h\|_{0,\Omega}, \forall\, q_h \in \mathbb{P}_h^1(\mathcal{T}_h). \tag{3.9}$$

Proof. Firstly, for any interior vertex O and its patch P_O, we can construct $\underset{\sim}{V}_{h0}^{\mathrm{sBDFM}}(P_O)$ and $\mathbb{P}_{h0}^1(P_O)$. Obviously div $\underset{\sim}{V}_{h0}^{\mathrm{sBDFM}}(P_O) \subset \mathbb{P}_{h0}^1(P_O)$. Thus by counting the dimension, we obtain div $\underset{\sim}{V}_{h0}^{\mathrm{sBDFM}}(P_O) = \mathbb{P}_{h0}^1(P_O)$ by Lemma 3.2. This verifies the condition (C_1) of Proposition 2.3.

The other conditions of Proposition 2.3 are direct, and the inf-sup condition holds by Proposition 2.3. The proof is completed. □

Now we consider the finite element discretization: Find $(\underset{\sim}{\varphi}_h, p_h) \in \underset{\sim}{V}_{h0}^{\mathrm{sBDFM}} \times \mathbb{P}_{h0}^1$, such that

$$\left\{\begin{array}{lcll} \varepsilon^2(\nabla_h \underset{\sim}{\varphi}_h, \nabla_h \underset{\sim}{\psi}_h) + (\operatorname{div} \underset{\sim}{\psi}_h, p_h) & = & (\underset{\sim}{f}, \underset{\sim}{\psi}_h), & \forall\, \underset{\sim}{\psi}_h \in \underset{\sim}{V}_{h0}^{\mathrm{sBDFM}} \\ (\operatorname{div} \underset{\sim}{\varphi}_h, q_h) & = & 0, & \forall\, q_h \in \mathbb{P}_{h0}^1. \end{array}\right. \tag{3.10}$$

The well-posedness of (3.10) is immediate.

Lemma 3.4. *Given* $\underset{\sim}{\varphi} \in \underset{\sim}{H}_0^1(\Omega) \cap \underset{\sim}{H}^2(\Omega)$ *such that* $\operatorname{div} \underset{\sim}{\varphi} = 0$*, it holds that*

$$\inf_{\underset{\sim}{\psi}_h \in \underset{\sim}{V}_{h0}^{\mathrm{sBDFM}},\, \operatorname{div} \underset{\sim}{\psi}_h = 0} \|\underset{\sim}{\varphi} - \underset{\sim}{\psi}_h\|_{1,h} \leqslant Ch\|\underset{\sim}{\varphi}\|_{2,\Omega}. \tag{3.11}$$

Proof. Let $(\underset{\sim}{\varphi}^*, p^*) \in \underset{\sim}{H}_0^1(\Omega) \times L_0^2(\Omega)$ be such that

$$\left\{\begin{array}{lcll} (\nabla \underset{\sim}{\varphi}^*, \nabla \underset{\sim}{\psi}) + (p^*, \operatorname{div} \underset{\sim}{\psi}) & = & (\operatorname{curl}\operatorname{rot} \underset{\sim}{\varphi}, \underset{\sim}{\psi}), & \forall\, \underset{\sim}{\psi} \in \underset{\sim}{H}_0^1(\Omega), \\ (\operatorname{div} \underset{\sim}{\varphi}^*, q) & = & 0, & \forall\, q \in L_0^2(\Omega). \end{array}\right. \tag{3.12}$$

Then $\underset{\sim}{\varphi}^* = \underset{\sim}{\varphi}$ and $p = 0$. Now let $(\underset{\sim}{\varphi}_h^*, p_h^*) \in \underset{\sim}{V}_{h0}^{\mathrm{sBDFM}} \times \mathbb{P}_{h0}^1$ be such that

$$\left\{\begin{array}{lcll} (\nabla_h \underset{\sim}{\varphi}_h^*, \nabla_h \underset{\sim}{\psi}_h) + (\operatorname{div} \underset{\sim}{\psi}_h, p_h^*) & = & (\operatorname{curl}\operatorname{rot} \underset{\sim}{\varphi}, \underset{\sim}{\psi}_h), & \forall\, \underset{\sim}{\psi}_h \in \underset{\sim}{V}_{h0}^{\mathrm{sBDFM}}, \\ (\operatorname{div} \underset{\sim}{\varphi}_h^*, q_h) & = & 0, & \forall\, q_h \in \mathbb{P}_{h0}^1. \end{array}\right. \tag{3.13}$$

Then $\operatorname{div} \underset{\sim}{\varphi}_h^* = 0$ and $\|\underset{\sim}{\varphi}^* - \underset{\sim}{\varphi}_h^*\| \leqslant Ch\|\underset{\sim}{\varphi}\|_{2,\Omega}$. The proof is completed. □

The convergence estimate robust in ε can be obtained in a standard way.

Theorem 3.5. *Let* $(\underset{\sim}{\varphi}, p)$ *and* $(\underset{\sim}{\varphi}_h, p_h)$ *be the solutions of* (1.4) *and* (3.10)*, respectively. If* $(\underset{\sim}{\varphi}, p) \in \underset{\sim}{H}^2(\Omega) \times H^1(\Omega)$*, then*

$$|\underset{\sim}{u} - \underset{\sim}{u}_h|_{1,h} \leqslant Ch|\underset{\sim}{u}|_{2,\Omega}, \quad \textit{and} \quad \|p - p_h\|_{0,\Omega} \leqslant C(h|p|_{1,\Omega} + \varepsilon^2 h|\underset{\sim}{u}|_{2,\Omega}). \tag{3.14}$$

4. A continuous nonconforming finite element scheme for the biharmonic equation

4.1. A finite element Stokes complex.

Define

$$V_h^{2+} := \{v_h \in H^1(\Omega) : v_h|_T \in P^{2+}(T),\ \forall\, T \in \mathcal{T}_h;\ \int_e \frac{\partial v_h}{\partial \mathbf{n}} \text{ is continuous across interior edge } e\}, \tag{4.1}$$

and

$$V_{h0}^{2+} := \{v_h \in V_h^{2+} \cap H_0^1(\Omega) : \int_e \frac{\partial v_h}{\partial \mathbf{n}} = 0 \text{ on boundary edge } e\}. \tag{4.2}$$

Lemma 4.1. *The exact sequence holds*

$$\{0\} \xrightarrow{\mathrm{inc}} V_{h0}^{2+} \xrightarrow{\mathrm{curl}} \underset{\sim}{V}_{h0}^{\mathrm{sBDFM}} \xrightarrow{\mathrm{div}} \mathbb{P}_{h0}^1 \xrightarrow{\int_\Omega \cdot} \{0\}. \tag{4.3}$$

Proof. Regarding Theorem 3.3, we only have to show

$$\{\underset{\sim}{v}_h \in \underset{\sim}{V}_{h0}^{\mathrm{sBDFM}} : \operatorname{div} \underset{\sim}{v}_h = 0\} = \operatorname{curl} V_{h0}^{2+}. \tag{4.4}$$

Denote $V_{h0}^{2+,C} := \{v_h \in H_0^1(\Omega) : v_h|_T \in P^{2+}(T),\ \forall\, T \in \mathcal{T}_h\}$. Given $\underset{\sim}{v}_h \in \underset{\sim}{V}_{h0}^{\mathrm{sBDFM}} \subset H_0(\mathrm{div}, \Omega)$ such that $\operatorname{div} \underset{\sim}{v}_h = 0$, by the local exact sequence Lemma 2.1 and the de Rham complex 1.1, there exists a $w_h \in V_{h0}^{2+,C}$, such that $\operatorname{curl} w_h = \underset{\sim}{v}_h$. Further, by the tangential continuity restriction on $\underset{\sim}{v}_h$, it follows that $w_h \in V_{h0}^{2+}$. The proof is completed. □

4.2. **A low-degree scheme for biharmonic equation.** We consider the biharmonic equation: given $g \in H^{-1}(\Omega)$, find $u \in H_0^2(\Omega)$, such that

$$(\nabla^2 u, \nabla^2 v) = \langle g, v\rangle, \quad \forall\, v \in H_0^2(\Omega). \tag{4.5}$$

A finite element discretization is to find $u_h \in V_{h0}^{2+}$, such that

$$(\nabla_h^2 u_h, \nabla_h^2 v_h) = \langle g, v_h\rangle, \quad \forall\, v_h \in V_{h0}^{2+}. \tag{4.6}$$

The lemma below is an immediate consequence of Lemmas 3.4 and 4.1.

Lemma 4.2. *It holds for $w \in H^3(\Omega) \cap H_0^2(\Omega)$ that*

$$\inf_{v_h \in V_{h0}^{2+}} \|w - v_h\|_{2,h} \leqslant Ch\|w\|_{3,\Omega}. \tag{4.7}$$

Proof. By Lemmas 4.1 and 3.4,

$$\begin{aligned} \inf_{v_h \in V_{h0}^{2+}} |w - v_h|_{2,h} &= \inf_{v_h \in V_{h0}^{2+}} |\operatorname{curl} w - \operatorname{curl} v_h|_{1,h} \\ &= \inf_{\underset{\sim}{\psi}_h \in \underset{\sim}{V}_{h0}^{\mathrm{sBDFM}},\ \operatorname{div} \underset{\sim}{\psi}_h = 0} |\operatorname{curl} w - \underset{\sim}{\psi}_h|_{1,h} \leqslant Ch|\operatorname{curl} w|_{2,\Omega} \leqslant Ch\|w\|_{3,\Omega}. \end{aligned} \tag{4.8}$$

This completes the proof. □

Theorem 4.3. *Let u and u_h be the solutions of* (4.5) *and* (4.6) *respectively, and assume $u \in H^3(\Omega) \cap H_0^2(\Omega)$. Then*

$$\|u - u_h\|_{2,h} \leqslant Ch\|u\|_{3,\Omega}. \tag{4.9}$$

The proof of the theorem follows from standard arguments, and we omit it here.

4.3. **Basis functions of V_{h0}^{2+}.** For the implementation of the finite element schemes, in this section, we present the explicit formulation of basis functions of certain finite element spaces.

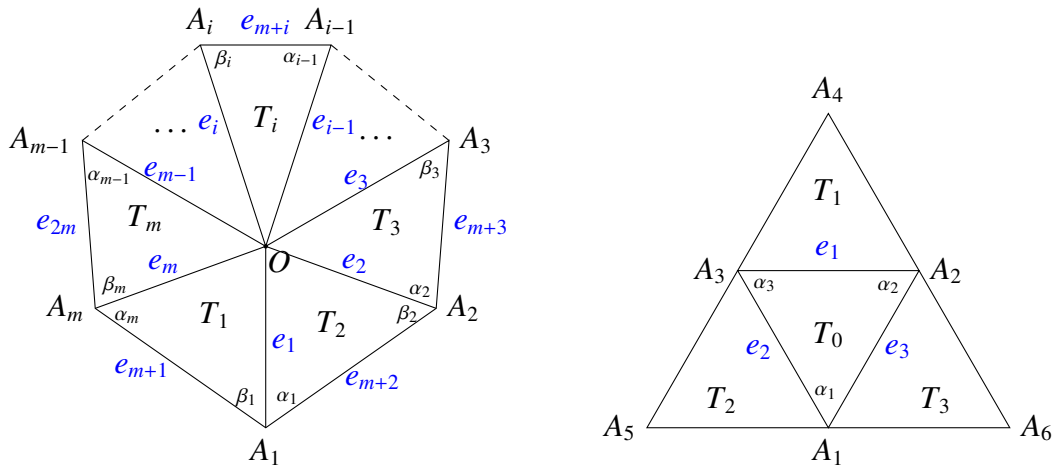

FIGURE 5. Illustration of a patch around O(left) and a patch around T_0(right).

4.3.1. *Basis function of the kernel subspace of* sBDFM *element.* Denote the kernel subspace

$$\underset{\sim}{Z}_{h0} := \{\underset{\sim}{v}_h \in \underset{\sim}{V}_{h0}^{\text{sBDFM}} : \operatorname{div} \underset{\sim}{v}_h = 0\}. \tag{4.10}$$

Firstly, associated with the interior vertex patch around an interior vertex O(cf. Figure 5, left), denote $\underset{\sim}{\psi}^O$ as

(4.11)

$$\underset{\sim}{\psi}^O = \begin{cases} \dfrac{d_{m+1}d_{m+2}\sin(\alpha_1+\beta_1)}{2(S_1+S_2)}\underset{\sim}{w}_{T_1,e_1} + \dfrac{d_{m+1}d_{2m}\sin(\alpha_m+\beta_m)}{2(S_1+S_m)}\underset{\sim}{w}_{T_1,e_m} + \underset{\sim}{w}_{T_1,e_1,e_m}, \ in\ T_1, \\ \dfrac{d_{m+i}d_{m+i+1}\sin(\alpha_i+\beta_i)}{2(S_i+S_{i+1})}\underset{\sim}{w}_{T_i,e_i} + \dfrac{d_{m+i}d_{m+i-1}\sin(\alpha_{i-1}+\beta_{i-1})}{2(S_i+S_{i-1})}\underset{\sim}{w}_{T_i,e_{i-1}} + \underset{\sim}{w}_{T_i,e_i,e_{i-1}}, \ in\ T_i (i=2:m-1), \\ \dfrac{d_{2m}d_{m+1}\sin(\alpha_m+\beta_m)}{2(S_m+S_1)}\underset{\sim}{w}_{T_m,e_m} + \dfrac{d_{2m}d_{2m-1}\sin(\alpha_{m-1}+\beta_{m-1})}{2(S_m+S_{m-1})}\underset{\sim}{w}_{T_m,e_{m-1}} + \underset{\sim}{w}_{T_m,e_m,e_{m-1}}, \ in\ T_m. \end{cases}$$

Secondly, associated with the interior cell patch around an interior cell T_0 (cf. Figure 5, right), denote $\underset{\sim}{\psi}_{T_0}$ as

(4.12)

$$\underset{\sim}{\psi}_{T_0} = \begin{cases} \dfrac{S_1}{S_1+S_0}\underset{\sim}{w}_{T_1,e_1}, \ in\ T_1, \\ \dfrac{S_2}{S_2+S_0}\underset{\sim}{w}_{T_2,e_2}, \ in\ T_2, \\ \dfrac{S_3}{S_3+S_0}\underset{\sim}{w}_{T_3,e_3}, \ in\ T_3, \\ \dfrac{1}{3}\Big(\dfrac{S_1-2S_0}{S_1+S_0}\underset{\sim}{w}_{T_0,e_1} + \dfrac{S_2-2S_0}{S_2+S_0}\underset{\sim}{w}_{T_0,e_2} + \dfrac{S_3-2S_0}{S_3+S_0}\underset{\sim}{w}_{T_0,e_3} + \underset{\sim}{w}_{T_0,e_2,e_3} + \underset{\sim}{w}_{T_0,e_3,e_1} + \underset{\sim}{w}_{T_0,e_1,e_2}\Big), \ in\ T_0. \end{cases}$$

Given an interior cell T_0 with vertices A_i, $i = 1:3$, and neighbored cells T_j, $j = 1:3$, the cell T_0 is covered by $\underset{\sim}{\psi}^{A_i}|_{T_0}$ for $i = 1:3$ and $\underset{\sim}{\psi}_{T_j}|_{T_0}$ for $j = 0:3$; see Figure 6 for an illustration. It is easy to know $\{\underset{\sim}{\psi}^{A_i}|_{T_0},\ i = 1:3,\ \underset{\sim}{\psi}_{T_j}|_{T_0},\ j = 0:3\}$ are linearly dependent. However, any six of them are linearly independent. For conciseness, we show the following lemma.

Lemma 4.4. *For an interior cell T_0 with vertices $A_i, i = 1:3$, and neighbored cells $T_j, j = 1:3$,(cf. Figure 6) the functions $\{\underset{\sim}{\psi}^{A_i}|_{T_0},\ i = 2:3,\ \underset{\sim}{\psi}_{T_j}|_{T_0},\ j = 0:3\}$ are linearly independent.*

Proof. A direct calculation leads to

$$\left(\underset{\sim}{\psi}^{A_2}|_{T_0}, \underset{\sim}{\psi}^{A_3}|_{T_0}, \underset{\sim}{\psi}_{T_0}|_{T_0}, \underset{\sim}{\psi}_{T_1}|_{T_0}, \underset{\sim}{\psi}_{T_2}|_{T_0}, \underset{\sim}{\psi}_{T_3}|_{T_0}\right)^\top = \mathbf{A}\left(\underset{\sim}{w}_{T_0,e_2,e_3}, \underset{\sim}{w}_{T_0,e_3,e_1}, \underset{\sim}{w}_{T_0,e_1,e_2}, \underset{\sim}{w}_{T_0,e_1}, \underset{\sim}{w}_{T_0,e_2}, \underset{\sim}{w}_{T_0,e_3}\right)^\top$$

$$\text{with } \mathbf{A} = \begin{bmatrix} 0 & 1 & 0 & \frac{d_2 d_5 \sin(\alpha_3+\gamma_3)}{2(S_1+S_0)} & 0 & \frac{d_2 d_8 \sin(\alpha_1+\beta_1)}{2(S_3+S_0)} \\ 0 & 0 & 1 & \frac{d_3 d_4 \sin(\alpha_2+\beta_2)}{2(S_1+S_0)} & \frac{d_3 d_7 \sin(\alpha_1+\gamma_1)}{2(S_2+S_0)} & 0 \\ \frac{1}{3} & \frac{1}{3} & \frac{1}{3} & \frac{S_1-2S_0}{3(S_1+S_0)} & \frac{S_2-2S_0}{3(S_2+S_0)} & \frac{S_3-2S_0}{3(S_3+S_0)} \\ 0 & 0 & 0 & \frac{S_0}{S_1+S_0} & 0 & 0 \\ 0 & 0 & 0 & 0 & \frac{S_0}{S_2+S_0} & 0 \\ 0 & 0 & 0 & 0 & 0 & \frac{S_0}{S_3+S_0} \end{bmatrix}.$$

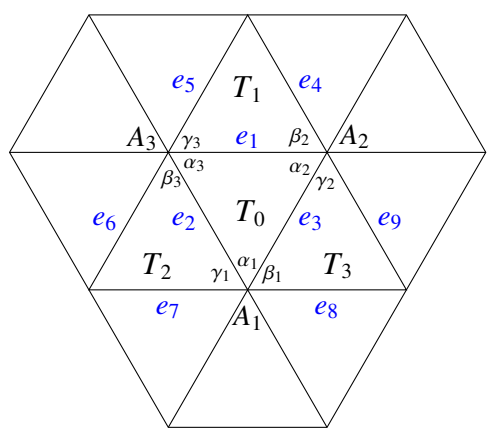

FIGURE 6. Illustration of all kernel basis functions upon one cell

As $\det(\mathbf{A}) = \dfrac{1}{3}\displaystyle\prod_{i=1:3} \dfrac{S_0}{S_0 + S_i}$ and $\left\{\underset{\sim}{w}_{T_0,e_2,e_3}, \underset{\sim}{w}_{T_0,e_3,e_1}, \underset{\sim}{w}_{T_0,e_1,e_2}, \underset{\sim}{w}_{T_0,e_1}, \underset{\sim}{w}_{T_0,e_2}, \underset{\sim}{w}_{T_0,e_3}\right\}$ are linearly independent, $\left\{\underset{\sim}{\psi}^{A_2}|_{T_0}, \underset{\sim}{\psi}^{A_3}|_{T_0}, \underset{\sim}{\psi}_{T_0}|_{T_0}, \underset{\sim}{\psi}_{T_1}|_{T_0}, \underset{\sim}{\psi}_{T_2}|_{T_0}, \underset{\sim}{\psi}_{T_3}|_{T_0}\right\}$ are linearly independent. □

Remark 4.5. *If a cell T_0 has one (or more) vertex aligned on the boundary, then it will be covered by no more than two interior vertex patches and be contained in supports of no more than six vertex- or cell-related kernel basis functions; the restriction of these six functions on T_0 are linearly independent.*

Lemma 4.6. *The functions of* $\Phi_h(\mathcal{T}_h) := \{\underset{\sim}{\psi}^A,\ A \in \mathcal{X}_h^i;\ \underset{\sim}{\psi}_T,\ T \in \mathcal{T}_h^i\}$ *form a basis of* $\underset{\sim}{Z}_{h0}$.

Proof. We only have to prove the functions of $\Phi_h(\mathcal{T}_h)$ are linearly independent. Indeed, provided that the set $\Phi_h(\mathcal{T}_h)$ is linearly independent, $\dim(\mathrm{span}(\Phi_h(\mathcal{T}_h))) = \#\mathcal{X}_h^i + \#\mathcal{T}_h^i = 3\#\mathcal{X}_h^i - 2 = 3\#\mathcal{E}_h^i - (3\#\mathcal{T}_h - 1) = \dim(\underset{\sim}{V}_{h0}^{\mathrm{sBDFM}}) - \dim(\mathbb{P}_{h0}^1) = \dim(\underset{\sim}{V}_{h0}^{\mathrm{sBDFM}}) - \dim(\mathrm{div}\,\underset{\sim}{V}_{h0}^{\mathrm{sBDFM}}) = \dim(\underset{\sim}{Z}_{h0})$, and thus $\underset{\sim}{Z}_{h0} = \mathrm{span}\,(\Phi_h(\mathcal{T}_h))$.

Now, given $\underset{\sim}{\psi}_h = \sum_{A\in\mathcal{X}_h^i} c_A\underset{\sim}{\psi}^A + \sum_{T\in\mathcal{T}_h^i} c_T\underset{\sim}{\psi}_T = 0$, we are going to show all c_A and c_T are zero. Similar to [36], we adopt a sweeping process here. Given $a \in \mathcal{X}_h^b$, let T be such that a is a vertex of T. Then

$$\underset{\sim}{\psi}_h|_T = \sum_{A\in\mathcal{X}_h^i\cap\overline{T}} c_A\underset{\sim}{\psi}^A|_T + \sum_{T'\in\mathcal{T}_h^i, T' \text{ and } T \text{ share a common edge}} c_{T'}\underset{\sim}{\psi}_{T'}|_T = 0.$$

By Lemma 4.4 and Remark 4.5, $c_A = 0$ for $A \in \mathcal{X}_h^i \cap \overline{T}$ and $c_{T'} = 0$ for $T' \in \mathcal{T}_h^i$, such that T' and T share a common edge. Therefore, $c_A = 0$ for any vertex $A \in \mathcal{X}_h^i$ that is connected to one boundary vertex $a \in \mathcal{X}_h^b$, and $c_T = 0$ for any $T \in \mathcal{T}_h^i$ that connects to a boundary vertex $a \in \mathcal{X}_h^b$. Similarly, we can show

$$c_A = 0\ \forall\, A \in \mathcal{X}_h^{b,+2}, \quad c_T = 0\ \forall\, T \in \mathcal{T}_h \text{ that connects to } \mathcal{X}_h^{b,+1}.$$

Repeating the procedure recursively, finally, we obtain

$$c_A = 0\ \forall\, A \in \mathcal{X}_h^{b,+k}, \quad c_T = 0\ \forall\, T \in \mathcal{T}_h \text{ that connects to } \mathcal{X}_h^{b,+(k-1)}$$

where k is the number of levels of the triangulation $\mathcal{T}_h$. Therefore, c_A and c_T are all zero and the functions of $\Phi_h(\mathcal{T}_h)$ are linearly independent. The proof is completed. □

4.3.2. *Basis functions of* V_{h0}^{2+}. Note that curl is a bijection from V_{h0}^{2+} onto $\underset{\sim}{Z}_{h0}$. Therefore, the basis functions of V_{h0}^{2+} are $\{\zeta^A,\ A \in \mathcal{X}_h^i;\ \zeta_T,\ T \in \mathcal{T}_h^i\}$, such that $\mathrm{curl}\,\zeta^A = \underset{\sim}{\psi}^A$ and $\mathrm{curl}\,\zeta_T = \underset{\sim}{\psi}_T$. More precisely(cf. Figure 5),

(4.13)

$$\zeta^O = \begin{cases} \lambda_0^2 + \dfrac{d_{m+1}d_{m+2}\sin(\alpha_1+\beta_1)}{2(S_1+S_2)}\lambda_0\lambda_1(3\lambda_m - 1) + \dfrac{d_{m+1}d_{2m}\sin(\alpha_m+\beta_m)}{2(S_1+S_m)}\lambda_0\lambda_m(3\lambda_1 - 1), \ \textit{in } T_1, \\ \lambda_0^2 + \dfrac{d_{m+i}d_{m+i+1}\sin(\alpha_i+\beta_i)}{2(S_i+S_{i+1})}\lambda_0\lambda_i(3\lambda_{i-1} - 1) + \dfrac{d_{m+i}d_{m+i-1}\sin(\alpha_{i-1}+\beta_{i-1})}{2(S_i+S_{i-1})}\lambda_0\lambda_{i-1}(3\lambda_i - 1), \ \textit{in } T_i, \\ \qquad\qquad\qquad\qquad\qquad\qquad\qquad\qquad\qquad\qquad\qquad\qquad (i = 2 : m-1) \\ \lambda_0^2 + \dfrac{d_{2m}d_{m+1}\sin(\alpha_m+\beta_m)}{2(S_m+S_1)}\lambda_0\lambda_m(3\lambda_{m-1} - 1) + \dfrac{d_{2m}d_{2m-1}\sin(\alpha_{m-1}+\beta_{m-1})}{2(S_m+S_{m-1})}\lambda_0\lambda_{m-1}(3\lambda_m - 1), \ \textit{in } T_m, \end{cases}$$

and

(4.14)

$$\zeta_{T_0} = \begin{cases} \dfrac{S_1}{S_1+S_0}\lambda_2\lambda_3(3\lambda_4-1), \ in\ T_1, \\ \dfrac{S_2}{S_1+S_0}\lambda_1\lambda_3(3\lambda_5-1), \ in\ T_2, \\ \dfrac{S_3}{S_1+S_0}\lambda_1\lambda_2(3\lambda_6-1), \ in\ T_3, \\ \dfrac{S_1}{S_1+S_0}\lambda_2\lambda_3(3\lambda_1-1)+\dfrac{S_2}{S_1+S_0}\lambda_1\lambda_3(3\lambda_2-1)+\dfrac{S_3}{S_1+S_0}\lambda_1\lambda_2(3\lambda_3-1)-6\lambda_1\lambda_2\lambda_3, \ in\ T_0. \end{cases}$$

5. An enriched linear − constant finite element scheme for incompressible flows

5.1. An enriched linear element space.

Define

$$\underset{\sim}{V}_h^{\mathrm{el}} := \{\underset{\sim}{v}_h \in H(\mathrm{div},\Omega) : \underset{\sim}{v}_h|_T \in \underset{\sim}{P}^{1+}(T),\ \int_e \underset{\sim}{v}_h\cdot\mathbf{t} \text{ is continuous across interior edge } e\},$$

and

$$\underset{\sim}{V}_{h0}^{\mathrm{el}} := \{\underset{\sim}{v}_h \in \underset{\sim}{V}_h^{\mathrm{el}} \cap H_0(\mathrm{div},\Omega) : \int_e \underset{\sim}{v}_h\cdot\mathbf{t} \text{ vanishes on boundary edge } e\}.$$

Remark 5.1. *Evidently,* $\underset{\sim}{V}_h^{\mathrm{el}} = \{\underset{\sim}{v}_h \in \underset{\sim}{V}_h^{\mathrm{sBDFM}} : \mathrm{div}\,\underset{\sim}{v}_h \in \mathbb{P}_{h0}^0\}$, *and* $\underset{\sim}{V}_{h0}^{\mathrm{el}} = \{\underset{\sim}{v}_h \in \underset{\sim}{V}_{h0}^{\mathrm{sBDFM}} : \mathrm{div}\,\underset{\sim}{v}_h \in \mathbb{P}_{h0}^0\}$. *Particularly,* $\{\underset{\sim}{v}_h \in \underset{\sim}{V}_{h0}^{\mathrm{el}} : \mathrm{div}\,\underset{\sim}{v}_h = 0\} = \{\underset{\sim}{v}_h \in \underset{\sim}{V}_{h0}^{\mathrm{sBDFM}} : \mathrm{div}\,\underset{\sim}{v}_h = 0\}$.

Lemma 5.2. *The exact sequence holds as*

$$\{0\} \to V_{h0}^{2+} \xrightarrow{\mathrm{curl}} \underset{\sim}{V}_{h0}^{\mathrm{el}} \xrightarrow{\mathrm{div}} \mathbb{P}_{h0}^0 \xrightarrow{\int_\Omega \cdot} \{0\}. \tag{5.1}$$

Lemma 5.3. *It can be verified that* $\underset{\sim}{V}_{h0}^{\mathrm{el}} = \underset{\sim}{V}_{h0}^{\mathrm{ZZZ}} \cap \underset{\sim}{V}_{h0}^{\mathrm{MTW}}$.

Proof. By definition, $\underset{\sim}{V}_{h0}^{\mathrm{el}} \subset \underset{\sim}{V}_{h0}^{\mathrm{sBDFM}} \subset \underset{\sim}{V}_{h0}^{\mathrm{ZZZ}}$ and $\underset{\sim}{V}_{h0}^{\mathrm{el}} \subset \underset{\sim}{V}_{h0}^{\mathrm{MTW}}$, namely $\underset{\sim}{V}_{h0}^{\mathrm{el}} \subset \underset{\sim}{V}_{h0}^{\mathrm{ZZZ}} \cap \underset{\sim}{V}_{h0}^{\mathrm{MTW}}$. On the other hand, given $\underset{\sim}{v}_h \in \underset{\sim}{V}_{h0}^{\mathrm{ZZZ}} \cap \underset{\sim}{V}_{h0}^{\mathrm{MTW}}$, $\underset{\sim}{v}_h|_T \in \underset{\sim}{P}_2(T)$, the normal component of $\underset{\sim}{v}_h|_T$ is piecewise linear, and $\mathrm{div}\,\underset{\sim}{v}_h|_T$ is a constant on T for any $T \in \mathcal{T}_h$; namely, $\underset{\sim}{v}_h|_T \in \underset{\sim}{P}^{1+}(T)$. Since all these three spaces $\underset{\sim}{V}_{h0}^{\mathrm{el}}$, $\underset{\sim}{V}_{h0}^{\mathrm{ZZZ}}$ and $\underset{\sim}{V}_{h0}^{\mathrm{MTW}}$ possess the same continuity, $\underset{\sim}{V}_{h0}^{\mathrm{el}} \supset \underset{\sim}{V}_{h0}^{\mathrm{ZZZ}} \cap \underset{\sim}{V}_{h0}^{\mathrm{MTW}}$. □

5.1.1. *Basis functions.* Firstly, we present associated with each edge $e \in \mathcal{E}_h^i$ a locally supported function $\underset{\sim}{\psi}_e$. Given $e \in \mathcal{E}_h^i$, it may happen that both ends of e are interior or that one end of e is on the boundary; see Figure 7 below.

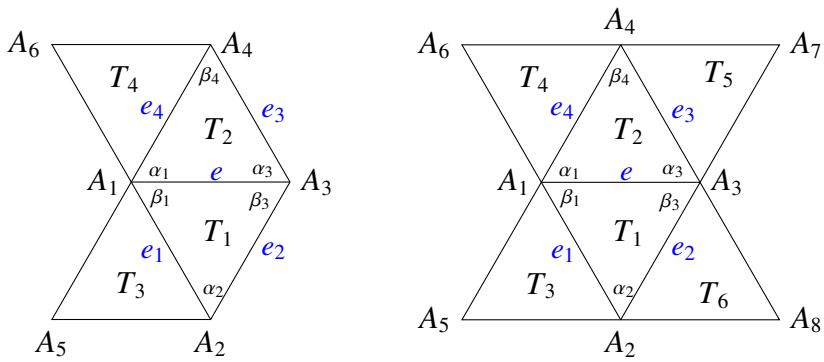

FIGURE 7. Illustration of basis functions associated with interior edges

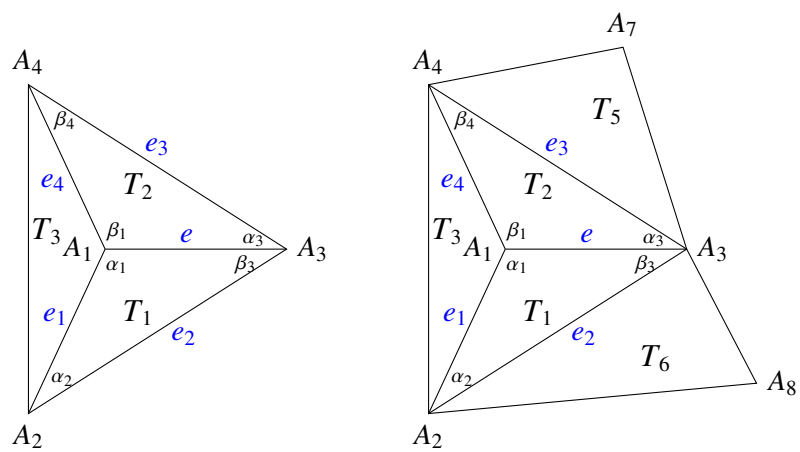

FIGURE 8. Two cases of degeneration; see Remark 5.4 below.

If e has a boundary vertex(e.g., in Figure 7(left), $A_1 \in \mathcal{X}_h^i, A_3 \in \mathcal{X}_h^b$), denote by

(5.2)

$$\underset{\sim}{\psi}_e := \begin{cases} \dfrac{S_3}{S_3+S_1}\underset{\sim}{w}_{T_3,e_1}, \ in\ T_3, \\ \underset{\sim}{y}_{T_1,e_1,e} + \dfrac{d_1\cos\alpha_2}{d_2}\underset{\sim}{w}_{T_1,e_1,e} + \dfrac{S_3}{S_3+S_1}\underset{\sim}{w}_{T_1,e_1} + \dfrac{\frac{1}{2}d_2d_3\sin(\alpha_3+\beta_3)-(S_1+S_2)}{S_1+S_2}\underset{\sim}{w}_{T_1,e}, \ in\ T_1, \\ -\underset{\sim}{y}_{T_2,e_4,e} + \dfrac{d_4\cos\alpha_4}{d_3}\underset{\sim}{w}_{T_2,e_4,e} + \dfrac{S_4}{S_4+S_2}\underset{\sim}{w}_{T_2,e_4} + \dfrac{\frac{1}{2}d_2d_3\sin(\alpha_3+\beta_3)-(S_1+S_2)}{S_1+S_2}\underset{\sim}{w}_{T_2,e}, \ in\ T_2, \\ \dfrac{S_4}{S_4+S_2}\underset{\sim}{w}_{T_4,e_4}, \ in\ T_4. \end{cases}$$

If both of the ends of e are interior vertices(e.g., in Figure 7(right), $A_1, A_3 \in \mathcal{X}_h^i$), denote by

(5.3)

$$\underset{\sim}{\psi}_e := \begin{cases} \dfrac{S_3}{2(S_3+S_1)}\underset{\sim}{w}_{T_3,e_1}, \ \textit{in } T_3, \\ \dfrac{S_4}{2(S_4+S_2)}\underset{\sim}{w}_{T_4,e_4}, \ \textit{in } T_4, \\ (\dfrac{S_3}{2(S_3+S_1)}-1)\underset{\sim}{w}_{T_1,e_1} + (1-\dfrac{S_6}{2(S_6+S_1)})\underset{\sim}{w}_{T_1,e_2} + \dfrac{\frac{1}{2}d_2d_3\sin(\alpha_3+\beta_3)-\frac{1}{2}d_1d_4\sin(\alpha_1+\beta_1)}{2(S_1+S_2)}\underset{\sim}{w}_{T_1,e} \\ \qquad\qquad + (\dfrac{d_2\cos\beta_3}{d}-\dfrac{1}{2})\underset{\sim}{w}_{T_1,e_1,e_2} + \dfrac{1}{2}\underset{\sim}{w}_{T_1,e_1,e} - \dfrac{1}{2}\underset{\sim}{w}_{T_1,e_2,e} + \underset{\sim}{y}_{T_1,e_1,e_2}, \ \textit{in } T_1, \\ (\dfrac{S_4}{2(S_4+S_2)}-1)\underset{\sim}{w}_{T_2,e_4} + (1-\dfrac{S_5}{2(S_5+S_2)})\underset{\sim}{w}_{T_2,e_3} + \dfrac{\frac{1}{2}d_2d_3\sin(\alpha_3+\beta_3)-\frac{1}{2}d_1d_4\sin(\alpha_1+\beta_1)}{2(S_1+S_2)}\underset{\sim}{w}_{T_2,e} \\ \qquad\qquad + (\dfrac{1}{2}-\dfrac{d_4\cos\beta_1}{d})\underset{\sim}{w}_{T_2,e_3,e_4} + \dfrac{1}{2}\underset{\sim}{w}_{T_2,e_4,e} - \dfrac{1}{2}\underset{\sim}{w}_{T_2,e_3,e} - \underset{\sim}{y}_{T_2,e_3,e_4}, \ \textit{in } T_2, \\ -\dfrac{S_5}{2(S_5+S_2)}\underset{\sim}{w}_{T_5,e_3}, \ \textit{in } T_5, \\ -\dfrac{S_6}{2(S_6+S_1)}\underset{\sim}{w}_{T_6,e_2}, \ \textit{in } T_6. \end{cases}$$

Remark 5.4. *It is still possible that the support of a basis function associated with an interior edge could cover exactly three or five cells. They can be viewed as the degenerated cases, and the function $\underset{\sim}{\psi}_e$ can be defined the same way. To be specific, when T_3 and T_4 coincide, the pattern in Figure 7(left) would degenerate to a patch with three cells as shown in Figure 8(left); moreover, $\underset{\sim}{\psi}_e|_{T_3} = \frac{S_3}{S_3+S_1}\underset{\sim}{w}_{T_3,e_1} + \frac{S_3}{S_3+S_2}\underset{\sim}{w}_{T_3,e_4}$ and $\underset{\sim}{\psi}_e|_{T_i}(i=1,2)$ are same to their counterparts in (5.2). Correspondingly, the pattern in Figure 7(right) would degenerate to a set of five cells as shown in Figure 8(right); $\underset{\sim}{\psi}_e|_{T_3} = \frac{S_3}{(2S_3+S_1)}\underset{\sim}{w}_{T_3,e_1} + \frac{S_3}{2(S_3+S_2)}\underset{\sim}{w}_{T_3,e_4}$ and $\underset{\sim}{\psi}_e|_{T_i}(i=1,2,5,6)$ keep counterparts as (5.3).*

Now we are going to show all these $\{\underset{\sim}{\psi}_e : \ e \in \mathcal{E}_h^i\}$ and $\{\underset{\sim}{\psi}_T : \ T \in \mathcal{T}_h^i\}$ form a basis of $\underset{\sim}{V}_{h0}^{\mathrm{el}}$.

Lemma 5.5. $\underset{\sim}{V}_{h0}^{\mathrm{el}} = \mathrm{span}\{\underset{\sim}{\psi}_e, \ e \in \mathcal{E}_h^i; \ \underset{\sim}{\psi}_T, \ T \in \mathcal{T}_h^i\}$.

Proof. Evidently, $\underset{\sim}{V}_{h0}^{\mathrm{el}} \supset \mathrm{span}\{\underset{\sim}{\psi}_e, \ e \in \mathcal{E}_h^i; \ \underset{\sim}{\psi}_T, \ T \in \mathcal{T}_h^i\}$. We turn to the other direction.

Firstly, we show $\mathrm{span}\{\mathrm{div}\,\underset{\sim}{\psi}_e, \ e \in \mathcal{E}_h^i\} = \mathbb{P}_{h0}^0$. For both cases as in Figure 7, $\mathrm{div}\,\underset{\sim}{\psi}_e = \frac{1}{S_1}$ on T_1 and $-\frac{1}{S_2}$ on T_2, and vanishes on all other cells. A simple algebraic argument leads to the assertion.

Secondly, all functions of $\underset{\sim}{Z}_{h0}$ can be represented by these functions. We only have to verify it for kernel functions each supported in a vertex patch. In fact, for an interior vertex O, $P_O = \cup_{i=1:m} T_i$,

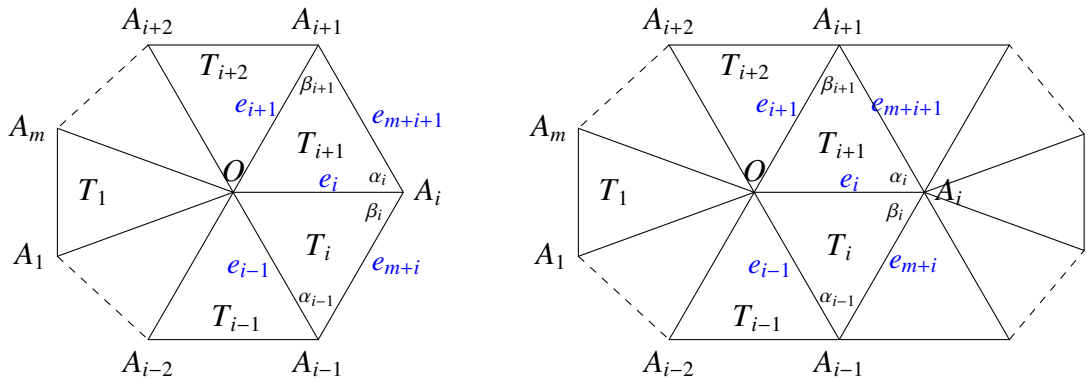

FIGURE 9. Illustration of the interior edge e_i with one(left) or two(right) interior vertices

$\overline{T}_i \cap \overline{T}_{i+1} = e_i$, $T_{m+1} = T_1$ and e_i connects O and A_i. Denote for $i = 1 : m$

$$\underset{\sim}{\psi}^*_{e_i} = \begin{cases} \underset{\sim}{\psi}_{e_i}, \ A_i \in \mathcal{X}^b_h, \\ \underset{\sim}{\psi}_{e_i} + \frac{1}{2}\underset{\sim}{\psi}_{T_i} + \frac{1}{2}\underset{\sim}{\psi}_{T_{i+1}}, \ A_i \in \mathcal{X}^i_h. \end{cases}$$

We refer to Figures 5 and 7, and formula (5.2), (5.3), (4.12) and(4.11) for the expressions of $\underset{\sim}{\psi}^O$, $\underset{\sim}{\psi}_{T_i}$ and $\underset{\sim}{\psi}_{e_i}$. Then, $\mathrm{supp}(\underset{\sim}{\psi}^*_{e_i}) = T_{i-1} \cup T_i \cup T_{i+1} \cup T_{i+2} \subset P_O$ in any event, and div $\sum_{i=1:m} \underset{\sim}{\psi}^*_{e_i} = 0$. Namely, $\sum_{i=1:m} \underset{\sim}{\psi}^*_{e_i} \in \underset{\sim}{Z}_O = \mathrm{span}\{\underset{\sim}{\psi}^O\}$. A further calculation leads to $\sum_{i=1:m} \underset{\sim}{\psi}^*_{e_i} = \underset{\sim}{\psi}^O$, namely

$$\underset{\sim}{\psi}^O = \sum_{i=1:m} \underset{\sim}{\psi}_{e_i} + \frac{1}{2} \sum_{i=1:m,\ A_i \in \mathcal{X}^i_h} (\underset{\sim}{\psi}_{T_i} + \underset{\sim}{\psi}_{T_{i+1}}). \tag{5.4}$$

Now, $\underset{\sim}{V}^{\mathrm{el}}_{h0}$ and $\mathrm{span}\{\underset{\sim}{\psi}_e,\ e \in \mathcal{E}^i_h;\ \underset{\sim}{\psi}_T,\ T \in \mathcal{T}^i_h\}$ have the same range under the operator div, and also $\underset{\sim}{Z}_{h0} \subset \mathrm{span}\{\underset{\sim}{\psi}_e,\ e \in \mathcal{E}^i_h;\ \underset{\sim}{\psi}_T,\ T \in \mathcal{T}^i_h\}$. Thus $\underset{\sim}{V}^{\mathrm{el}}_{h0} = \mathrm{span}\{\underset{\sim}{\psi}_e,\ e \in \mathcal{E}^i_h;\ \underset{\sim}{\psi}_T,\ T \in \mathcal{T}^i_h\}$.

Further, $\dim(\mathrm{span}\{\underset{\sim}{\psi}_e,\ e \in \mathcal{E}^i_h;\ \underset{\sim}{\psi}_T,\ T \in \mathcal{T}^i_h\}) = \dim(\underset{\sim}{V}^{\mathrm{el}}_{h0}) = \dim(\underset{\sim}{Z}_{h0}) + \dim(\mathbb{P}^0_{h0}) = \#\mathcal{X}^i_h + \#\mathcal{T}^i_h + \#\mathcal{T}_h - 1 = \#\mathcal{T}^i_h + \#\mathcal{E}^i_h = \#(\{\underset{\sim}{\psi}_e,\ e \in \mathcal{E}^i_h;\ \underset{\sim}{\psi}_T,\ T \in \mathcal{T}^i_h\})$. Therefore, the functions $\{\underset{\sim}{\psi}_e,\ e \in \mathcal{E}^i_h;\ \underset{\sim}{\psi}_T,\ T \in \mathcal{T}^i_h\}$ are linearly independent, and they form a set of basis of $\underset{\sim}{V}^{\mathrm{el}}_{h0}$. The proof is completed. □

5.2. **A lowest degree conservative scheme for the Stokes equation.** Denote

$$\mathbb{P}^0_h(\mathcal{T}_h) := \{q_h \in L^2(\Omega) : q_h|_T \in P_0(T), \forall\, T \in \mathcal{T}_h\} \text{ and } \mathbb{P}^0_{h0}(\mathcal{T}_h) := \mathbb{P}^0_h(\mathcal{T}_h) \cap L^2_0(\Omega).$$

Based on the new finite element, a discretization scheme of (1.3) is: Find $(\underset{\sim}{u}_h, p_h) \in \underset{\sim}{V}_{h0}^{\mathrm{el}} \times \mathbb{P}_{h0}^0$, such that

$$\begin{cases} \varepsilon^2(\nabla_h \underset{\sim}{u}_h, \nabla_h \underset{\sim}{v}_h) - (\operatorname{div} \underset{\sim}{v}_h, p_h) & = (\underset{\sim}{f}, \underset{\sim}{v}_h), \quad \forall\, \underset{\sim}{v}_h \in \underset{\sim}{V}_{h0}^{\mathrm{el}}, \\ (\operatorname{div} \underset{\sim}{u}_h, q_h) & = 0, \qquad \forall\, q_h \in \mathbb{P}_{h0}^0. \end{cases} \tag{5.5}$$

Lemma 5.6 (Stability of $\underset{\sim}{V}_{h0}^{\mathrm{el}} - \mathbb{P}_{h0}^0$)**.** *It holds uniformly that*

$$\inf_{q_h \in \mathbb{P}_{h0}^0} \sup_{\underset{\sim}{v}_h \in \underset{\sim}{V}_{h0}^{\mathrm{el}}} \frac{(\operatorname{div} \underset{\sim}{v}_h, q_h)}{\|q_h\|_{0,\Omega} \|\underset{\sim}{v}_h\|_{1,h}} \geqslant C > 0. \tag{5.6}$$

Proof. Given $q_h \in \mathbb{P}_{h0}^0 \subset \mathbb{P}_{h0}^1$, there exists $\underset{\sim}{v}_h \in \underset{\sim}{V}_{h0}^{\mathrm{sBDFM}}$, such that $\|\underset{\sim}{v}_h\|_{1,h} \leqslant C\|q_h\|_{0,\Omega}$ and $\operatorname{div} \underset{\sim}{v}_h = q_h$, which implies $\underset{\sim}{v}_h \in \underset{\sim}{V}_{h0}^{\mathrm{el}}$. The proof is completed. □

Lemma 5.7. *Given* $\underset{\sim}{w} \in \underset{\sim}{H}^2(\Omega)$*, it holds that*

$$\inf_{\underset{\sim}{v}_h \in \underset{\sim}{V}_h^{\mathrm{el}}} \|\underset{\sim}{w} - \underset{\sim}{v}_h\|_{1,h} \leqslant Ch\|\underset{\sim}{w}\|_{2,\Omega}. \tag{5.7}$$

Given $\underset{\sim}{w} \in \underset{\sim}{H}^2(\Omega) \cap \underset{\sim}{H}_0^1(\Omega)$ *such that* $\operatorname{div} \underset{\sim}{w} = 0$*, it holds that*

$$\inf_{\underset{\sim}{v}_h \in \underset{\sim}{V}_{h0}^{\mathrm{sBDFM}},\, \operatorname{div} \underset{\sim}{v}_h = 0} \|\underset{\sim}{w} - \underset{\sim}{v}_h\|_{1,h} \leqslant Ch\|\underset{\sim}{w}\|_{2,\Omega}. \tag{5.8}$$

Proof. Since linear element space is contained in $\underset{\sim}{V}_{h0}^{\mathrm{el}}$, (5.7) holds directly. From Lemma 3.4 and Remark 5.1, (5.8) follows. The proof is completed. □

The system (5.5) is uniformly well-posed by Brezzi's theory as below.

Lemma 5.8. *The problem* (5.5) *admits a unique solution pair* $(\underset{\sim}{u}_h, p_h)$*, and*

$$\varepsilon\|\underset{\sim}{u}_h\|_{1,h} + \frac{1}{\varepsilon}\|p_h\|_{0,\Omega} \eqsim \frac{1}{\varepsilon}\|\underset{\sim}{f}\|_{-1,h}, \tag{5.9}$$

where $\|\underset{\sim}{f}\|_{-1,h} := \sup_{\underset{\sim}{v}_h \in \underset{\sim}{V}_{h0}^{\mathrm{el}}} \frac{(\underset{\sim}{f}, \underset{\sim}{v}_h)}{\|\underset{\sim}{v}_h\|_{1,h}}$.

Proof. We only have to verify Brezzi's condition with respect to the parametrized norms. □

Theorem 5.9. *Let* $(\underset{\sim}{u}, p)$ *and* $(\underset{\sim}{u}_h, p_h)$ *be the solutions of* (1.4) *and* (5.5)*, respectively. If* $\underset{\sim}{u} \in \underset{\sim}{H}^2(\Omega)$ *and* $p \in H^1(\Omega)$*, then*

$$\|\underset{\sim}{u} - \underset{\sim}{u}_h\|_{1,h} \leqslant Ch\|\underset{\sim}{u}\|_{2,\Omega}, \quad \|p - p_h\|_{0,\Omega} \leqslant Ch(\varepsilon^2\|\underset{\sim}{u}\|_{2,\Omega} + \|p\|_{1,\Omega}). \tag{5.10}$$

Here the constant C does not depend on the parameter ε*.*

Proof. The argument is quite standard, and we omit the details here. We only have to note that, since the scheme is strictly conservative, the solution of $\underset{\sim}{u}$ can be completely separated from p, and Lemma 5.7 works here. □

Remark 5.10. *A further reduction of $\underset{\sim}{V}_h^{\mathrm{el}}$ leads to the spaces*

$$\underset{\sim}{V}_h^1 := \{\underset{\sim}{v}_h \in H(\mathrm{div},\Omega) : \ \underset{\sim}{v}_h|_T \in \underset{\sim}{P}_1(T),\ \forall\, T \in \mathcal{T},\ \int_e \underset{\sim}{v}_h \cdot \mathbf{t} \text{ is continuous across } e \in \mathcal{E}_h^i\} \tag{5.11}$$

and

$$\underset{\sim}{V}_{h0}^1 := \{\underset{\sim}{v}_h \in \underset{\sim}{V}_h^1 \cap H_0(\mathrm{div},\Omega),\ \int_e \underset{\sim}{v}_h \cdot \mathbf{t} = 0 \text{ on boundary edges } e \in \mathcal{E}_h^b\}. \tag{5.12}$$

The pair $\underset{\sim}{V}_{h0}^1 - \mathbb{P}_{h0}^0$ may be viewed as the most natural, if not the only, $\underset{\sim}{P}_1 - P_0$ pair for the Stokes problem. Generally, this pair is not stable; we refer to Appendix A for a numerical verification. This way, we view the $\underset{\sim}{V}_{h0}^{\mathrm{el}} - \mathbb{P}_{h0}^0$ pair as a **lowest-degree** *stable conservative pair for the Stokes problem on general triangulations.*

6. Numerical phenomena for eigenvalue problems

In this section, we test the numerical performance of the scheme for the Stokes eigenvalue problem: find $(\underset{\sim}{u}, p) \in \underset{\sim}{H}_0^1(\Omega) \times L_0^2(\Omega)$, such that

$$\begin{cases} \varepsilon^2(\nabla \underset{\sim}{u}, \nabla \underset{\sim}{v}) - (\mathrm{div}\, \underset{\sim}{v}, p) &= \lambda(\underset{\sim}{u}, \underset{\sim}{v}), \quad \forall\, \underset{\sim}{v} \in \underset{\sim}{H}_0^1(\Omega), \\ (\mathrm{div}\, \underset{\sim}{u}, q) &= 0, \qquad \forall\, q \in L_0^2(\Omega). \end{cases} \tag{6.1}$$

Note that the two pairs ($\underset{\sim}{V}_{h0}^{\mathrm{sBDFM}} - \mathbb{P}_{h0}^1$ and $\underset{\sim}{V}_{h0}^{\mathrm{el}} - \mathbb{P}_{h0}^0$) lead to same computed eigenvalues on same grids. Series of numerical experiments are carried out and the computed eigenvalues are recorded below. For every example, we show the domain and initial grid in the left, and a list of computed values of the six lowest eigenvalues in the right. For these examples, we choose $\varepsilon = 1$.

Example 1.

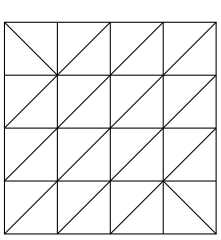

Mesh	0	1	2	3	4	Trend
λ_1	66.4097	55.5965	53.1347	52.5407	52.3936	↘
λ_2	123.5251	99.7536	94.0682	92.6136	92.2471	↘
λ_3	137.3504	104.5997	95.1729	92.8802	92.3129	↘
λ_4	165.0641	145.8915	132.8618	129.3819	128.5035	↘
λ_5	201.2460	181.6767	161.1576	155.8845	154.5653	↘
λ_6	203.7052	196.9708	174.6248	168.9307	167.5051	↘

Example 2.

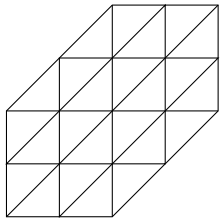

Mesh	0	1	2	3	4	Trend
λ_1	86.6443	83.3799	81.4757	80.9330	80.7931	$\searrow$
λ_2	137.7299	113.2535	105.8261	103.8102	103.2968	$\searrow$
λ_3	186.2746	177.2660	157.0575	151.3276	149.9012	$\searrow$
λ_4	219.7048	179.7712	171.8289	170.2635	169.8594	$\searrow$
λ_5	225.8015	216.8896	204.0614	199.9510	198.8708	$\searrow$
λ_6	247.3904	269.6167	223.8862	211.9163	208.9613	$\searrow$

Example 3.

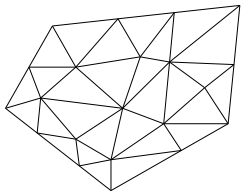

Mesh	0	1	2	3	4	Trend
λ_1	25.8121	23.3012	22.4095	22.1664	22.1039	$\searrow$
λ_2	42.4798	37.8163	35.2351	34.5166	34.3322	$\searrow$
λ_3	52.0032	46.2567	43.5630	42.8074	42.6114	$\searrow$
λ_4	62.4579	61.7980	55.8809	54.1927	53.7558	$\searrow$
λ_5	70.0038	66.4962	60.3462	58.6252	58.1810	$\searrow$
λ_6	83.8312	82.6286	75.2565	72.9644	72.3525	$\searrow$

Example 4.

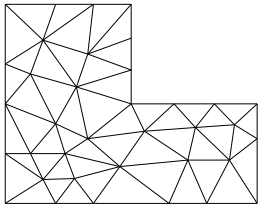

Mesh	0	1	2	3	4	Trend
λ_1	36.5520	33.5002	32.4349	32.1805	32.1302	$\searrow$
λ_2	48.3991	39.8558	37.7611	37.2135	37.0697	$\searrow$
λ_3	53.0517	45.0956	42.7302	42.1349	41.9870	$\searrow$
λ_4	60.3236	53.6852	50.2220	49.2993	49.0633	$\searrow$
λ_5	63.4514	60.6123	56.8284	55.7646	55.4969	$\searrow$
λ_6	79.9487	76.4633	71.4214	69.9839	69.6178	$\searrow$

Example 5.

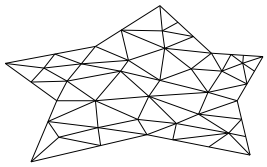

Mesh	0	1	2	3	4	Trend
λ_1	27.0359	25.1845	24.5809	24.4196	24.3798	$\searrow$
λ_2	48.0933	44.7486	42.9104	42.4146	42.2914	$\searrow$
λ_3	51.0107	44.8693	43.1253	42.6689	42.5528	$\searrow$
λ_4	73.8299	64.1797	60.4715	59.4812	59.2282	$\searrow$
λ_5	82.0255	69.5011	65.2793	64.1854	63.9103	$\searrow$
λ_6	92.5390	84.0946	78.2179	76.6211	76.2141	$\searrow$

It can be observed according to the experiments that

- the computed eigenvalues converge to a limit in the speed of $O(h^2)$;
- the computed eigenvalues decrease as the mesh is refined, which implies that the computed eigenvalues provide upper bounds of the exact eigenvalues.

7. Concluding remarks

In this paper, a new conservative pair $\underset{\sim}{V}^{\mathrm{el}}_{h0} - \mathbb{P}^0_{h0}$ is established and shown stable for incompressible Stokes problem, and a numerical verification as in Appendix A illustrates that the $\underset{\sim}{V}^{\mathrm{el}}_{h0} - \mathbb{P}^0_{h0}$

pair is a lowest-degree one that is stable and conservative on general triangulations. The velocity component has an appearance of $H(\mathrm{div})$ element added with divergence-free bubble functions, and is comparable with ones given in, e.g., [10, 20, 28]. However, the finite element space for velocity does not correspond to a Ciarlet's triple, and the construction and theoretical analysis can not be carried out in a usual way. The main technical ingredient is then to use an indirect approach by constructing and utilizing an auxiliary pair $\underset{\sim}{V}_{h0}^{\mathrm{sBDFM}} - \mathbb{P}_{h0}^{1}$.

The auxiliary pair $\underset{\sim}{V}_{h0}^{\mathrm{sBDFM}} - \mathbb{P}_{h0}^{1}$ is constructed by reducing $H(\mathrm{div})$ finite element spaces which was firstly adopted in [30]. It is interesting to notice that, the sBDFM element has the same nodal parameters as ones given in [20, 28] (the lowest-degree) and [10] (the lowest-degree), but it uses the lowest-degree polynomials among these four, and only the sBDFM element space can accompany the piecewise linear polynomial space to form a stable pair, while the other three can only accompany the piecewise constant space.

Besides, for conservative pairs in three-dimension, we refer to, e.g., [12, 31, 35] where composite grids are required, as well as [13] and [34] where high degree local polynomials are utilized. We refer to [7, 17, 33] for pairs on rectangular grids and [21] for ones on cubic grids where full advantage of the geometric symmetry of the cells are taken. The approaches given in [30] and the present paper can be generalized to higher dimensions and non-simplicial grids. This will be discussed in future.

Finally, it is worthy of noticing that, the finite element schemes given in the present paper, when used for the Stokes eigenvalue problem, can provide upper bounds for the exact eigenvalues. It has not been reported in the literature that nonconforming finite element schemes may provide upper bounds for the Stokes eigenvalue problem. In this paper, this unexpected phenomenon is illustrated by plenty of numerical experiments. Theoretical and further numerical investigation will be carried out in future.

Appendix A. A most natural linear–constant pair is not stable: a numerical verification

In this section, we show by numerics the $\underset{\sim}{V}_{h0}^{1} - \mathbb{P}_{h0}^{0}$, defined in Remark 5.10, is not stable on general triangulations, whereas

$$\inf_{q_h \in \mathrm{div}\, \underset{\sim}{V}_{h0}^{1}} \sup_{\underset{\sim}{v}_h \in \underset{\sim}{V}_{h0}^{1}} \frac{(\mathrm{div}\, \underset{\sim}{v}_h, q_h)}{\|q_h\|_{0,\Omega} |\underset{\sim}{v}_h|_{1,h}} = O(h) \tag{A.1}$$

on a specific kind of triangulations.

A.1. **A special triangulation and finite element space.** We consider the computational domain $\Omega = (0,1)\times(0,1)\setminus(\{(x,y): 0\leqslant x\leqslant \frac{1}{2}, x+\frac{1}{2}\leqslant y\leqslant 1\}\cup\{(x,y): \frac{1}{2}\leqslant x\leqslant 1, 0\leqslant y\leqslant x-\frac{1}{2}\})$. The initial triangulation is shown in Figure 10(left), and a sequence of triangulations are obtained by refining it uniformly(cf. Figure 10(right)).

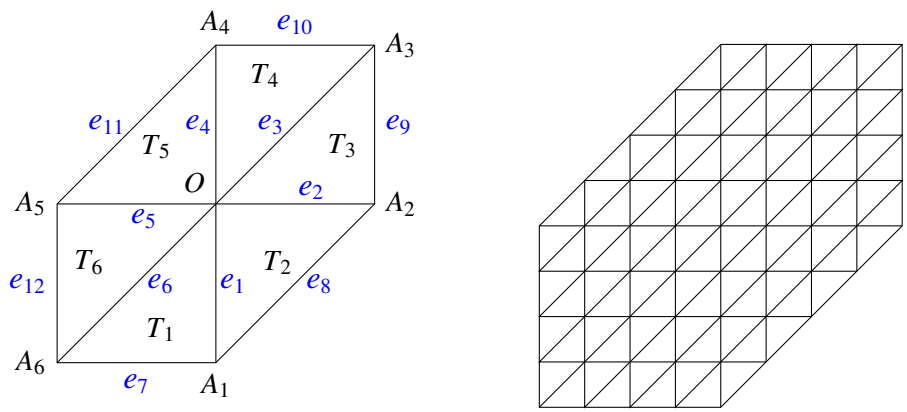

FIGURE 10. Left: the initial grid or a 6-cell patch. Right: the grid after twice refinement

Given a patch P_O as shown in Figure 10(left), denote by $\underset{\sim}{V}^1_{h0}(P_O) = \text{span}\{\underset{\sim}{\varphi}^O_1, \underset{\sim}{\varphi}^O_2, \underset{\sim}{\varphi}^O_3\}$ and denote for $i = 1:6$, $\underset{\sim}{V}^1_{h0}(T_i) = \text{span}\{\underset{\sim}{\varphi}^1_{T_i}, \underset{\sim}{\varphi}^2_{T_i}, \underset{\sim}{\varphi}^3_{T_i}\}$. Specifically, $\underset{\sim}{\varphi}^O_s|_{T_i} = \underset{\sim}{\varphi}^s_{T_i}$, $s = 1:2, i = 1:6$ and

$$\underset{\sim}{\varphi}^O_3 = \begin{cases} \underset{\sim}{\varphi}^1_{T_1} - 2\underset{\sim}{\varphi}^2_{T_1} + \underset{\sim}{\varphi}^2_{T_1}, \ in\ T_1; & \underset{\sim}{\varphi}^1_{T_2} - \underset{\sim}{\varphi}^2_{T_2} - \underset{\sim}{\varphi}^2_{T_2}, \ in\ T_2; \\ 2\underset{\sim}{\varphi}^1_{T_3} - \underset{\sim}{\varphi}^2_{T_3} + \underset{\sim}{\varphi}^2_{T_3}, \ in\ T_3; & \underset{\sim}{\varphi}^1_{T_4} - 2\underset{\sim}{\varphi}^2_{T_4} + \underset{\sim}{\varphi}^2_{T_4}, \ in\ T_4; \\ \underset{\sim}{\varphi}^1_{T_5} - \underset{\sim}{\varphi}^2_{T_5} - \underset{\sim}{\varphi}^2_{T_5}, \ in\ T_5; & 2\underset{\sim}{\varphi}^1_{T_6} - \underset{\sim}{\varphi}^2_{T_6} + \underset{\sim}{\varphi}^2_{T_6}, \ in\ T_6; \end{cases} \tag{A.2}$$

where for $i = 1:6$, $\underset{\sim}{\varphi}^1_{T_i} = \begin{pmatrix} \lambda_0 \\ 0 \end{pmatrix}$, $\underset{\sim}{\varphi}^2_{T_i} = \begin{pmatrix} 0 \\ \lambda_0 \end{pmatrix}$, and $\underset{\sim}{\varphi}^3_{T_1} = \begin{pmatrix} \lambda_6 - \lambda_1 \\ 0 \end{pmatrix}$, $\underset{\sim}{\varphi}^3_{T_2} = \begin{pmatrix} \lambda_1 - \lambda_2 \\ \lambda_1 - \lambda_2 \end{pmatrix}$, $\underset{\sim}{\varphi}^3_{T_3} = \begin{pmatrix} 0 \\ \lambda_2 - \lambda_3 \end{pmatrix}$, $\underset{\sim}{\varphi}^3_{T_4} = \begin{pmatrix} \lambda_3 - \lambda_4 \\ 0 \end{pmatrix}$, $\underset{\sim}{\varphi}^3_{T_5} = \begin{pmatrix} \lambda_4 - \lambda_5 \\ \lambda_4 - \lambda_5 \end{pmatrix}$, $\underset{\sim}{\varphi}^3_{T_6} = \begin{pmatrix} 0 \\ \lambda_5 - \lambda_6 \end{pmatrix}$.

Similar to Lemma 4.6, we can show the lemma below.

Lemma A.1. *dim*$(\underset{\sim}{V}^1_{h0}) = 3\#\mathcal{X}^i_h$ *and* $\underset{\sim}{V}^1_{h0} = \text{span}\{\underset{\sim}{\varphi}^A_1, \underset{\sim}{\varphi}^A_2, \underset{\sim}{\varphi}^A_3, A\in\mathcal{X}^i_h\}$.

A.2. **Numerical verification of the inf-sup constant.** By Courant's min-max theorem, it is easy to show the lemma below.

Lemma A.2. *With respect to any set of basis functions of* $\underset{\sim}{V}^1_{h0}$ *and* $\mathbb{P}^0_h$*, denote by A the stiffness matrix of* $(\nabla_h\cdot, \nabla_h\cdot)$ *on* $\underset{\sim}{V}^1_{h0}$*, by M the mass matrix on* $\underset{\sim}{V}^1_{h0}$*, and by B the stiffness matrix of* $(\text{div}\cdot, \cdot)$

on $\underset{\sim}{V}^1_{h0} \times \mathbb{P}^0_h$. *Then*

$$\inf_{q_h \in \operatorname{div} \underset{\sim}{V}^1_{h0}} \sup_{\underset{\sim}{v}_h \in \underset{\sim}{V}^1_{h0}} \frac{(\operatorname{div} \underset{\sim}{v}_h, q_h)}{\|q_h\|_{0,\Omega} |\underset{\sim}{v}_h|_{1,h}} = \lambda^+_{\min},$$

where $\lambda^+_{\min}$ *is the smallest positive eigenvalue of the matrix eigenvalue problem* $BA^{-1}B^T \mathrm{v} = \lambda M \mathrm{v}$.

The maximum eigenvalue of the proposed eigenvalue problem is denoted by $\lambda_{\max}$. Table 1 displays the computed values of $\lambda^+_{\min}$ and $\lambda_{\max}$ on a series of refined grids. And Figure 11 illustrates that $\lambda^+_{\min}$ degenerates in the rate of $O(h)$. This verifies (A.1) numerically.

h	$\lambda^+_{\min}$	Rate	$\lambda_{\max}$
1/2	0.2232	-	1.3822
1/4	0.1235	0.8538	1.4081
1/8	0.0636	0.9574	1.4131
1/16	0.0321	0.9865	1.4140
1/32	0.0161	0.9955	1.4142
1/64	0.0081	0.9911	1.4142

TABLE 1. Computed values of $\lambda^+_{\min}$ and $\lambda_{\max}$

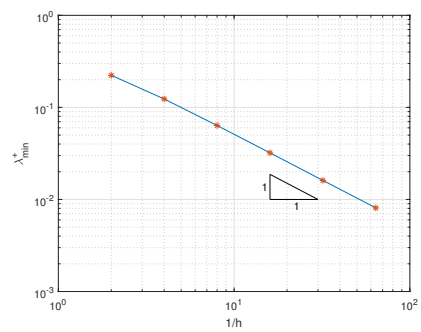

FIGURE 11. λ^+_{min} decays along with mesh refinement

REFERENCES

[1] Douglas Arnold. *Finite Element Exterior Calculus*. SIAM, 2018.

[2] Douglas Arnold, Richard Falk, and Ragnar Winther. Finite element exterior calculus, homological techniques, and applications. *Acta Numerica*, 15:1–155, 2006.

[3] Douglas N. Arnold and Jinshui Qin. Quadratic velocity/linear pressure Stokes elements. In *Advances in Computer Methods for Partial Differential Equations VII*, pages 28–34. IMACS, 1992.

[4] F. Auricchio, L. Beirão da Veiga, C. Lovadina, and A. Reali. The importance of the exact satisfaction of the incompressibility constraint in nonlinear elasticity: mixed FEMs versus NURBS-based approximations. *Computer Methods in Applied Mechanics and Engineering*, 199(5):314–323, 2010. Computational Geometry and Analysis.

[5] Ferdinando Auricchio, Lourenço Beirão da Veiga, Carlo Lovadina, Alessandro Reali, Robert L. Taylor, and Peter Wriggers. Approximation of incompressible large deformation elastic problems: some unresolved issues. *Computational Mechanics*, 52(5):1153–1167, 2013.

[6] Franco Brezzi, Michel Fortin, and SpringerLink. *Mixed and Hybrid Finite Element Methods*, volume 15. Springer New York, New York, 1991.

[7] ShaoChun Chen, LiNa Dong, and ZhongHua Qiao. Uniformly convergent H(div)-conforming rectangular elements for Darcy–Stokes problem. *Science China Mathematics*, 56(12):2723–2736, 2013.

[8] Richard S. Falk and Michael Neilan. Stokes complexes and the construction of stable finite elements with pointwise mass conservation. *SIAM Journal on Numerical Analysis*, 51(2):1308–1326, 2013.

[9] Nicolas R. Gauger, Alexander Linke, and Philipp W. Schroeder. On high-order pressure-robust space discretisations, their advantages for incompressible high reynolds number generalised Beltrami flows and beyond. *SMAI Journal of Computational Mathematics*, 5:89–129, 2019.

[10] Johnny Guzman and Michael Neilan. A family of nonconforming elements for the Brinkman problem. *IMA Journal of Numerical Analysis*, 32(4):1484–1508, 2012.

[11] Johnny Guzmán and Michael Neilan. Conforming and divergence-free Stokes elements on general triangular meshes. *Mathematics of Computation*, 83(285):15–36, 2014.

[12] Johnny Guzmán and Michael Neilan. Inf-sup stable finite elements on barycentric refinements producing divergence–free approximations in arbitrary dimensions. *SIAM Journal on Numerical Analysis*, 56(5):2826–2844, 2018.

[13] Johnny Guzmán and Michael Neilan. Conforming and divergence-free Stokes elements in three dimensions. *IMA Journal of Numerical Analysis*, 34:1489–1508, 10 2013.

[14] Ralf Hiptmair, Lingxiao Li, Shipeng Mao, and Weiying Zheng. A fully divergence-free finite element method for magnetohydrodynamic equations. *Mathematical Models and Methods in Applied Sciences*, pages 1–37, 2018.

[15] Kaibo Hu, Yicong Ma, and Jinchao Xu. Stable finite element methods preserving $\nabla \cdot \mathbf{B} = 0$ exactly for MHD models. *Numerische Mathematik*, 135(2):371–396, 2017.

[16] Kaibo Hu and Jinchao Xu. Structure-preserving finite element methods for stationary MHD models. *Mathematics of Computation*, 88(316):553–581, 03 2019.

[17] Yunqing Huang and Shangyou Zhang. A lowest order divergence-free finite element on rectangular grids. *Frontiers of Mathematics in China*, 6(002):253–270, 2011.

[18] Volker John, Alexander Linke, Christian Merdon, Michael Neilan, and Leo G Rebholz. On the divergence constraint in mixed finite element methods for incompressible flows. *SIAM Review*, 59(3):492–544, 2017.

[19] Alexander Linke and Christian Merdon. Well-balanced discretisation for the compressible Stokes problem by gradient-robustness. In Robert Klöfkorn, Eirik Keilegavlen, Florin A. Radu, and Jürgen Fuhrmann, editors, *Finite Volumes for Complex Applications IX - Methods, Theoretical Aspects, Examples*, pages 113–121, Cham, 2020. Springer International Publishing.

[20] Kent Andre Mardal, Xue-Cheng Tai, and Ragnar Winther. A robust finite element method for Darcy–Stokes flow. *SIAM Journal on Numerical Analysis*, 40(5):1605–1631, 2002.

[21] Michael Neilan and Duygu Sap. Stokes elements on cubic meshes yielding divergence-free approximations. *Calcolo*, 53(3):263–283, 2016.

[22] Jinshui Qin and Shangyou Zhang. Stability and approximability of the $P_1 - P_0$ element for Stokes equations. *International Journal for Numerical Methods in Fluids*, 54(5):497–515, 2007.

[23] Philipp Schroeder and Gert Lube. Divergence-free H(div)-FEM for time-dependent incompressible flows with applications to high reynolds number vortex dynamics. *Journal of Scientific Computing*, 75:830–858, 05 2018.

[24] L. R. Scott and M. Vogelius. Norm estimates for a maximal right inverse of the divergence operator in spaces of piecewise polynomials. *EAIRO - Modélisation Mathématique et Analyse Numérique*, 19(1):111–143, 1985.

[25] Rolf Stenberg. A technique for analysing finite element methods for viscous incompressible flow. *International Journal for Numerical Methods in Fluids*, 11(6):935–948, 1990.

[26] Xue–Cheng Tai and Ragnar Winther. A discrete de Rham complex with enhanced smoothness. *Calcolo*, 43(4):287–306, 2006.

[27] Shinya Uchiumi. A viscosity-independent error estimate of a pressure-stabilized Lagrange-Galerkin scheme for the Oseen problem. *Journal of Scientific Computing*, 80(2):834–858, 2019.

[28] Xiaoping Xie, Jinchao Xu, and Guangri Xue. Uniformly stable finite element methods for Darcy–Stokes–Brinkman models. *Journal of Computational Mathematics*, 26:437–455, 05 2008.

[29] Xuejun Xu and Shangyou Zhang. A new divergence-free interpolation operator with applications to the Darcy–Stokes–Brinkman equations. *SIAM Journal on Scientific Computing*, 32(2):855–874, 2010.

[30] Huilan Zeng, Chensong Zhang, and Shuo Zhang. A low-degree strictly conservative finite element method for incompressible flows. *arXiv: 2103.00705*, 2021.

[31] Shangyou Zhang. A new family of stable mixed finite elements for the 3D Stokes equations. *Mathematics of computation*, 74(250):543–554, 2005.

[32] Shangyou Zhang. On the P_1 Powell-Sabin divergence-free finite element for the Stokes equations. *Journal of Computational Mathematics*, 26(003):456–470, 2008.

[33] Shangyou Zhang. A family of $Q_{k+1,k} \times Q_{k,k+1}$ divergence-free finite elements on rectangular grids. *SIAM Journal on Numerical Analysis*, 47(3):2090–2107, 01 2009.

[34] Shangyou Zhang. Divergence-free finite elements on tetrahedral grids for $k \geqslant 6$. *Mathematics of Computation*, 80(274):669–695, 2011.

[35] Shangyou Zhang. Quadratic divergence-free finite elements on Powell–Sabin tetrahedral grids. *Calcolo*, 48(3):211–244, September 2011.

[36] Shuo Zhang. Minimal consistent finite element space for the biharmonic equation on quadrilateral grids. *IMA Journal of Numerical Analysis*, 40(2):1390–1406, 2020.

[37] Shuo Zhang. An optimal piecewise cubic nonconforming finite element scheme for the planar biharmonic equation on general triangulation. *Science China Mathematics*, accepted, 2021.

LSEC, Institute of Computational Mathematics and Scientific/Engineering Computing, Academy of Mathematics and System Sciences, Chinese Academy of Sciences, Beijing 100190; University of Chinese Academy of Sciences, Beijing, 100049; People's Republic of China

Email address: {wjliu,szhang}@lsec.cc.ac.cn